Zwitterionic λ^5*Si*-Organofluorosilicates of the Formula Types $F_4SiCH_2NMe_2R$ and $F_3MeSiCH_2NMe_2R$ (R = H, Me) and Related Compounds: Synthesis, Structure, and Dynamic Behavior†

Reinhold Tacke,*,‡ Joachim Becht,‡ Olaf Dannappel,‡ Reinhart Ahlrichs,§ Uwe Schneider,§ William S. Sheldrick,|| Josef Hahn,⊥ and Frank Kiesgen⊥

Institut für Anorganische Chemie, Universität Würzburg, Am Hubland, D-97074 Würzburg, Germany, Lehrstuhl für Theoretische Chemie, Institut für Physikalische Chemie und Elektrochemie, Universität Karlsruhe, Engesserstrasse, Geb. 30.43, D-76128 Karlsruhe, Germany, Lehrstuhl für Analytische Chemie, Ruhr-Universität Bochum, Universitätsstrasse 150, D-44780 Bochum, Germany, and Institut für Anorganische Chemie, Universität Köln, Greinstrasse 6, D-50939 Köln, Germany

Received December 4, 1995⊗

The zwitterionic λ^5*Si*-organofluorosilicates $F_4SiCH_2NMe_2H$ (**5**) and $F_3MeSiCH_2NMe_2H$ (**7**; crystallographic modifications **7a** and **7b**) were synthesized by reaction of the silanes $(MeO)_3SiCH_2NMe_2$ (**11**) and $(MeO)_2MeSiCH_2NMe_2$ (**13**), respectively, with HF in a mixture of ethanol and hydrofluoric acid at 0 °C. The related zwitterionic λ^5*Si*-organofluorosilicates $F_4SiCH_2NMe_3$ (**6**) and $F_3MeSiCH_2NMe_3$ (**8**) were obtained analogously by reaction of HF with the ammonium iodides $[(MeO)_3SiCH_2NMe_3]I$ (**12**) and $[(MeO)_2MeSiCH_2NMe_3]I$ (**14**), respectively. Reaction of the silanes $(MeO)_3SiCH_2NR_2$ (**16**) and $(MeO)_2{}^tBuSiCH_2NR_2$ (**17**) (NR_2 = 2,2,6,6-tetramethylpiperidino) with HF gave the zwitterionic λ^5*Si*-organofluorosilicates $F_4SiCH_2NR_2H$ (**9**) and $F_3{}^tBuSiCH_2NR_2H$ (**10**), respectively. The crystal structures of compounds **5**, **6**, **7a**,**b**, and **8**−**10** were determined by single-crystal X-ray diffraction studies. Compounds **5**−**10** were studied by solution-state ^1H, ^{13}C, ^{19}F, and ^{29}Si NMR experiments at room temperature (solvent CD_3CN). These studies indicate a rapid fluorine exchange at room temperature. As shown by temperature-dependent ^{19}F NMR experiments with **10** (solvent CD_2Cl_2), this ligand exchange can be reduced on cooling. According to line-shape analyses, the dynamic behavior of **10** can be described by two different processes. For compounds **5**−**8** and related model species ab initio studies at the SCF/SVP and MP2/TZP levels were performed. Calculated and experimental (crystal structures) geometric data were compared, and the influence of intermolecular interactions (packing effects) in the solid state and intramolecular interactions between the charged centers in the calculated zwitterions were studied. Furthermore, the dynamic behavior of the title compounds was investigated by ab initio studies of the related model species $F_4SiCH_2NH_3$ (**19**) and $F_3MeSiCH_2NH_3$ (**20**).

Introduction

The study of compounds of pentacoordinate silicon is currently one of the main areas of research in silicon chemistry.[1] In the past few years, we have contributed to this field with a series of systematic investigations on novel zwitterionic λ^5*Si*-silicates,[2] such as the molecular λ^5*Si*-organofluorosilicates **1**,[2e] **2**,[2i] **3**,[2j] and **4**.[2j] The zwitterionic framework of these compounds is characterized by the presence of a pentacoordinate (formally negatively charged) silicon atom and a tetracoordinate (formally positively charged) nitrogen atom (in this context, see also refs 3 and 4).

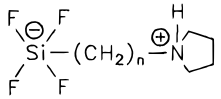

1: n = 1
2: n = 2

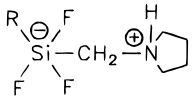

3: R = Me
4: R = Ph

In continuation of these studies,[2] we addressed the basic problem of how the coordination polyhedra around the silicon atoms of such compounds are affected by intra- and intermolecular interactions. For this purpose, the zwitterionic λ^5*Si*-organofluorosilicates **5**−**10** were synthesized and their crystal structures determined by single-crystal X-ray diffraction studies. Furthermore, quantum-mechanical methods[5] were applied (for theoretical studies on pentacoordinate silicon spe-

* To whom correspondence should be addressed.
† Dedicated to Professor Ernst Mutschler on the occasion of his 65th birthday.
‡ Universität Würzburg.
§ Universität Karlsruhe.
|| Ruhr-Universität Bochum.
⊥ Universität Köln.
⊗ Abstract published in *Advance ACS Abstracts,* March 1, 1996.

(1) Reviews on the chemistry of pentacoordinate silicon: (a) Tandura, S. N.; Voronkov, M. G.; Alekseev, N. V. *Top. Curr. Chem.* **1986**, *131*, 99−189. (b) Sheldrick, W. S. In *The Chemistry of Organic Silicon Compounds*; Patai, S., Rappoport, Z., Eds.; Wiley: Chichester, U.K., 1989; Part 1, pp 227−303. (c) Corriu, R. J. P.; Young, J. C. In *The Chemistry of Organic Silicon Compounds*; Patai, S., Rappoport, Z., Eds.; Wiley: Chichester, U.K., 1989; Part 2, pp 1241−1288. (d) Holmes, R. R. *Chem. Rev.* **1990**, *90*, 17−31. (e) Chuit, C.; Corriu, R. J. P.; Reye, C.; Young, J. C. *Chem. Rev.* **1993**, *93*, 1371−1448. (f) Wong, C. Y.; Woollins, J. D. *Coord. Chem. Rev.* **1994**, *130*, 175−241.

0276-7333/96/2315-2060$12.00/0

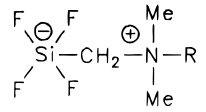

5: R = H
6: R = Me

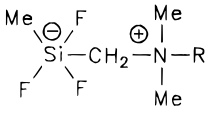

7: R = H
8: R = Me

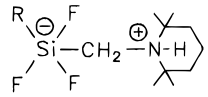

9: R = F
10: R = ^{t}Bu

cies, see refs 6−8; see also ref 9) and the calculated and experimental geometric data compared.

A second topic of this work concerns investigations of the dynamic behavior of the title compounds. For this purpose, NMR studies and theoretical calculations were performed in order to determine pathways for an intramolecular ligand exchange and the energetic barriers for these processes.

Results and Discussion

Syntheses. The zwitterionic tetrafluorosilicates **5** and **6** were synthesized according to Scheme 1, starting from [(dimethylamino)methyl]trimethoxysilane[2g] (**11**). Reaction of **11** with HF gave [(dimethylammonio)-methyl]tetrafluorosilicate (**5**), and N-quaternization of **11** with methyl iodide in acetonitrile and subsequent reaction of the resulting ammonium salt **12** (crude product, not characterized) with HF yielded tetrafluoro-[(trimethylammonio)methyl]silicate (**6**). The reactions **11** → **5** and **12** → **6** were carried out in a mixture of 40% hydrofluoric acid and ethanol at 0 °C. After recrystallization from methanol or acetonitrile (0 → −30 °C), compounds **5** and **6** were isolated in 83% and 87% yields (relative to **11**), respectively.

The trifluorosilicates **7** and **8** were prepared analogously to **5** and **6**, starting from [(dimethylamino)-methyl]dimethoxy(methyl)silane[2g] (**13**) (Scheme 2). Reaction of **13** with HF yielded [(dimethylammonio)-methyl]trifluoro(methyl)silicate (**7**), and N-quaternization of **13** with methyl iodide in acetonitrile and subsequent reaction of the resulting ammonium salt **14** (crude product, not characterized) with HF gave trifluoro(methyl)[(trimethylammonio)methyl]silicate (**8**). The reactions **13** → **7** and **14** → **8** again were carried out in a mixture of 40% hydrofluoric acid and ethanol at 0 °C. Upon recrystallization from methanol (0 → −30 °C), compounds **7** (crystallographic modification **7a**) and **8** were obtained in 72% and 81% yields (relative to **13**), respectively. In addition, crystals of a second modification of **7** (crystallographic modification **7b**) could be obtained by recrystallization from ethanol (40 → 20 °C).

Tetrafluoro[(2,2,6,6-tetramethylpiperidinio)methyl]-silicate (**9**) and *tert*-butyltrifluoro[(2,2,6,6-tetramethylpiperidinio)methyl]silicate (**10**) were prepared from (chloromethyl)trimethoxysilane[10] (**15**) according to Scheme 3. In the first step, the silane **15** was transformed into trimethoxy[(2,2,6,6-tetramethylpiperidino)-methyl]silane (**16**) by treatment with neat 2,2,6,6-tetramethylpiperidine (yield 64%). Subsequent reaction of **16** with *tert*-butyllithium in *n*-pentane gave *tert*-butyldimethoxy[(2,2,6,6-tetramethylpiperidino)methyl]-silane (**17**) (yield 64%). The silanes **16** and **17** were then transformed into the respective zwitterionic silicates **9**

Scheme 1

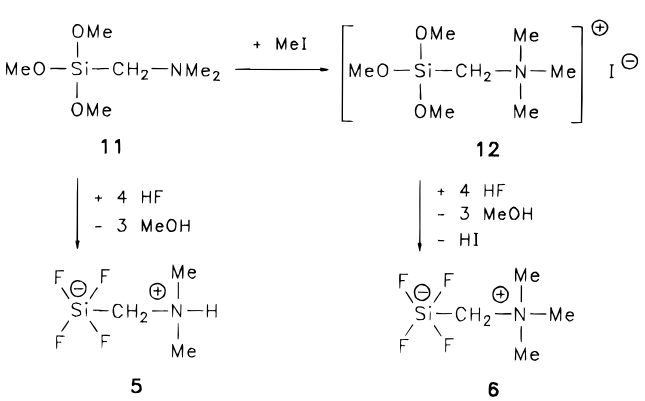

(2) (a) Strohmann, C.; Tacke, R.; Mattern, G.; Kuhs, W. F. *J. Organomet. Chem.* **1991**, *403*, 63−71. (b) Tacke, R.; Sperlich, J.; Strohmann, C.; Mattern, G. *Chem. Ber.* **1991**, *124*, 1491−1496. (c) Tacke, R.; Sperlich, J.; Strohmann, C.; Frank, M.; Mattern, G. *Z. Kristallogr.* **1992**, *199*, 91−98. (d) Tacke, R.; Wiesenberger, F.; Lopez-Mras, A.; Sperlich, J.; Mattern, G. *Z. Naturforsch., B* **1992**, *47*, 1370−1376. (e) Tacke, R.; Becht, J.; Mattern, G.; Kuhs, W. F. *Chem. Ber.* **1992**, *125*, 2015−2018. (f) Tacke, R.; Lopez-Mras, A.; Sheldrick, W. S.; Sebald, A. *Z. Anorg. Allg. Chem.* **1993**, *619*, 347−358. (g) Tacke, R.; Lopez-Mras, A.; Sperlich, J.; Strohmann, C.; Kuhs, W. F.; Mattern, G.; Sebald, A. *Chem. Ber.* **1993**, *126*, 851−861. (h) Sperlich, J.; Becht, J.; Mühleisen, M.; Wagner, S. A.; Mattern, G.; Tacke, R. *Z. Naturforsch., B* **1993**, *48*, 1693−1706. (i) Tacke, R.; Lopez-Mras, A.; Becht, J.; Sheldrick, W. S. *Z. Anorg. Allg. Chem.* **1993**, *619*, 1012−1016. (j) Tacke, R.; Becht, J.; Lopez-Mras, A.; Sheldrick, W. S.; Sebald, A. *Inorg. Chem.* **1993**, *32*, 2761−2766. (k) Tacke, R.; Becht, J.; Lopez-Mras, A.; Sperlich, J. *J. Organomet. Chem.* **1993**, *446*, 1−8. (l) Tacke, R.; Lopez-Mras, A.; Jones, P. G. *Organometallics* **1994**, *13*, 1617−1623. (m) Tacke, R.; Mühleisen, M.; Jones, P. G. *Angew. Chem.* **1994**, *106*, 1250−1252; *Angew. Chem., Int. Ed. Engl.* **1994**, *33*, 1186−1188. (n) Mühleisen, M.; Tacke, R. *Chem. Ber.* **1994**, *127*, 1615−1617. (o) Tacke, R.; Mühleisen, M. *Inorg. Chem.* **1994**, *33*, 4191−4193. (p) Mühleisen, M.; Tacke, R. *Organometallics* **1994**, *13*, 3740−3742. (q) Tacke, R.; Becht, J.; Dannappel, O.; Kropfgans, M.; Lopez-Mras, A.; Mühleisen, M.; Sperlich, J. In *Progress in Organosilicon Chemistry*; Marciniec, B., Chojnowski, J., Eds.; Gordon and Breach: Amsterdam, 1995; pp 55−68. (r) Tacke, R.; Mühleisen, M.; Lopez-Mras, A.; Sheldrick, W. S. *Z. Anorg. Allg. Chem.* **1995**, *621*, 779−788. (s) Tacke, R.; Dannappel, O.; Mühleisen, M. In *Organosilicon Chemistry II*; Auner, N., Weis, J., Eds.; VCH: Weinheim, Germany, 1996; pp 427−446.

(3) Publications on related anionic λ^5Si species of the type $[F_4SiR]^-$ (R = organic substituent): (a) Müller, R. *Organomet. Chem. Rev.* **1966**, *1*, 359−377. (b) Schomburg, D. *J. Organomet. Chem.* **1981**, *221*, 137−141. (c) Johnson, S. E.; Day, R. O.; Holmes, R. R. *Inorg. Chem.* **1989**, *28*, 3182−3189.

(4) Publications on related anionic λ^5Si species of the type $[F_3SiR_2]^-$ (R = organic substituent): (a) Schomburg, D.; Krebs, R. *Inorg. Chem.* **1984**, *23*, 1378−1381. (b) Damrauer, R.; Danahey, S. E. *Organometallics* **1986**, *5*, 1490−1494. (c) Harland, J. J.; Payne, J. S.; Day, R. O.; Holmes, R. R. *Inorg. Chem.* **1987**, *26*, 760−765. (d) Johnson, S. E.; Payne, J. S.; Day, R. O.; Holmes, J. M.; Holmes, R. R. *Inorg. Chem.* **1989**, *28*, 3190−3198. (e) Johnson, S. E.; Deiters, J. A.; Day, R. O.; Holmes, R. R. *J. Am. Chem. Soc.* **1989**, *111*, 3250−3258. (f) Day, R. O.; Sreelatha, C.; Deiters, J. A.; Johnson, S. E.; Holmes, J. M.; Howe, L.; Holmes, R. R. *Organometallics* **1991**, *10*, 1758−1766. (g) Tamao, K.; Hayashi, T.; Ito, Y. *Organometallics* **1992**, *11*, 182−191. (h) Kira, M.; Hoshi, T.; Kabuto, C.; Sakurai, H. *Chem. Lett.* **1993**, 1859−1862.

(5) To the best of our knowledge, compounds **5**−**8** represent the smallest neutral λ^5Si species synthesized and characterized so far. Thus, it was very likely to study these species by both experimental and theoretical methods.

(6) Theoretical studies concerning the nature of the chemical bond in anionic pentacoordinate silicon species: (a) Cahill, P. A.; Dykstra, C. E.; Martin, J. C. *J. Am. Chem. Soc.* **1985**, *107*, 6359−6366. (b) Albright, T. A.; Burdett, J. K.; Wangboo, M. *Orbital Interactions in Chemistry*; Wiley: New York, 1985; pp 258−276. (c) O'Keeffe, M. *J. Am. Chem. Soc.* **1986**, *108*, 4341−4343. (d) Sakai, S.; Imoto, M. *J. Mol. Struct. (THEOCHEM)* **1989**, *187*, 317−323. (e) Gordon, M. S.; Davis, L. P.; Burggraf, L. W. *Chem. Phys. Lett.* **1989**, *163*, 371−374. (f) Deiters, J. A.; Holmes, R. R. *J. Am. Chem. Soc.* **1990**, *112*, 7197−7202. (g) Fujimoto, H.; Yabuki, T.; Tamao, K.; Fukui, K. *J. Mol. Struct. (THEOCHEM)* **1992**, *260*, 47−61.

Scheme 2

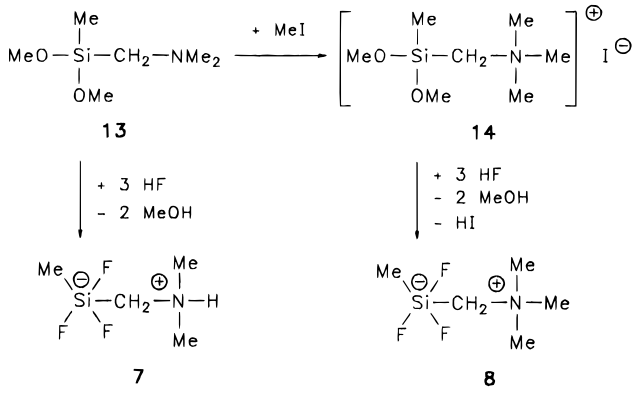

Scheme 3

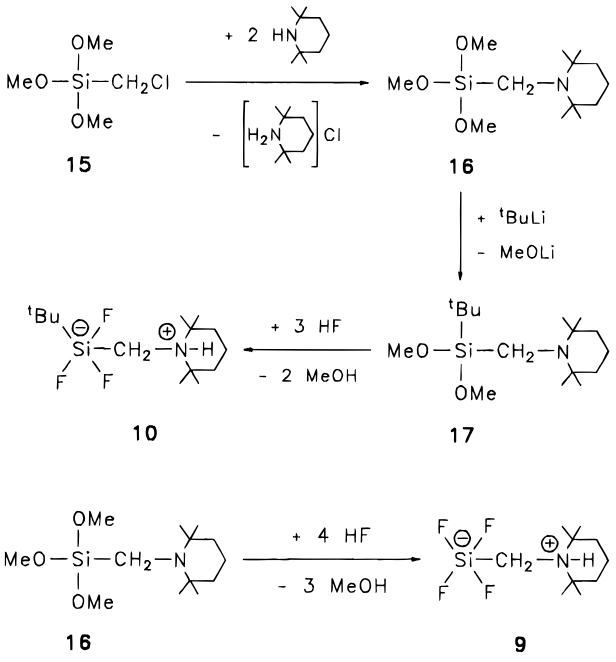

and **10** by reaction with HF in a mixture of 40% hydrofluoric acid and ethanol at 0 °C. Upon recrystallization from acetonitrile (0 → −30 °C), the latter compounds were obtained in 95% and 68% yields, respectively.

The title compounds **5**−**10** were isolated as colorless, crystalline solids, which are almost insoluble in nonpolar organic solvents and also exhibit a rather poor solubility in polar organic solvents. The identities of **5**−**10** were established by elemental analyses (C, H, F, N), multinuclear solution-state NMR studies (^{1}H, ^{13}C, ^{19}F, ^{29}Si), and mass-spectrometric investigations (EI MS or FD MS). In addition, compounds **5**, **6**, and **10** were characterized by solid-state ^{29}Si CP/MAS NMR experiments, and the crystal structures of **5**, **6**, **7a**,**b**, and **8**−**10** were studied by single-crystal X-ray diffraction.

Crystal Structure Analyses. The crystal structures of compounds **5**, **6**, **7a**,**b**, and **8**−**10** were determined by single-crystal X-ray diffraction studies. The crystal data and experimental parameters used for these experiments are given in Tables 1−3 (for further details, see Experimental Section). The molecular structures of the zwitterions **5**−**10** in the crystal are shown in Figures 1−6. Selected interatomic distances and angles are listed in Tables 4−7.

For all compounds studied, the geometry of the coordination polyhedron around the silicon atom can be described as a distorted trigonal bipyramid (TBP). In all zwitterions the two axial positions are occupied by fluorine atoms (F(1) and F(2)). As may be gathered from the bond distances and angles, all molecules display similar deviations from the idealized TBP, the greatest deviations being observed for **10**. The observed distortions are not in accordance with angular movements on the Berry-pseudorotation pathway toward a square-pyramidal geometry.

The equatorial bond angles in the trifluorosilicates **7a**,**b**, **8**, and **10** reflect the greater steric requirements of the organic groups (methyl or *tert*-butyl) in comparison to the fluorine atom in the tetrafluorosilicates **5**, **6**, and **9** and the weaker polarization of the Si−C bond in comparison to the Si−F bond. As a consequence, the deviations of the sum of the equatorial bond angles in the trifluorosilicates from the ideal value of 360° are greater than those observed for the related tetrafluorosilicates. As a further consequence, the C(1)−Si−C(2) angles in the trifluorosilicates are enlarged to values of >120°, accompanied by a concomitant narrowing of the F(3)−Si−C(1) and F(3)−Si−C(2) angles to values of <120° (e.g. compound **10**: F(3)−Si−C(1) = 113.9(1)°, F(3)−Si−C(2) = 118.5(1)°, C(1)−Si−C(2) = 127.5(1)°). The axial bond angles F(1)−Si−F(2) also deviate from the ideal value of 180° (minimum deviation 179.7(1)° (**9**); maximum deviation 172.4(1)° (**10**)), and the F_{ax}−Si−F_{eq} and F_{ax}−Si−C_{eq} angles deviate from the ideal value of 90° (minimum deviation 90.06(8)° (**5**, molecule 1); maximum deviation 96.5(2)° (**6**)). The deformation parameter Δ,[4c] defined as the sum of the axial and equatorial bond angle displacements from the ideal values of 180 and 120°, varies in a range between 3.7 and 15.1° (angles used for these calculations: F(1)−Si−F(2) and the equatorial angle with the greatest deviation from the ideal value of 120° (tetrafluorosilicates); F(1)−Si−F(2) and C(1)−Si−C(2) (trifluorosilicates)). Similar Δ values have been reported for related ionic tetra- and trifluorosilicates, for instance 6.8 and 12.4° for the

(7) Theoretical studies concerning transition states or intermediates in S_N2 reactions at silicon: (a) Anh, N. T.; Minot, C. *J. Am. Chem. Soc.* **1980**, *102*, 103−107. (b) Dewar, M. J. S.; Healy, E. *Organometallics* **1982**, *1*, 1705−1708. (c) Sheldon, J. C.; Hayes, R. N.; Bowie, J. H. *J. Am. Chem. Soc.* **1984**, *106*, 7711−7715. (d) Davis, L. P.; Burggraf, L. W.; Gordon, M. S.; Baldridge, K. K. *J. Am. Chem. Soc.* **1985**, *107*, 4415−4419. (e) Gordon, M. S.; Davis, L. P.; Burggraf, L. W.; Damrauer, R. *J. Am. Chem. Soc.* **1986**, *108*, 7889−7893. (f) Sheldon, J. C.; Hayes, R. N.; Bowie, J. H.; DePuy, C. H. *J. Chem. Soc., Perkin Trans. 2* **1987**, 275−280. (g) Deiters, J. A.; Holmes, R. R. *J. Am. Chem. Soc.* **1987**, *109*, 1686−1692. (h) Deiters, J. A.; Holmes, R. R. *J. Am. Chem. Soc.* **1987**, *109*, 1692−1696. (i) Davis, L. P.; Burggraf, L. W.; Gordon, M. S. *J. Am. Chem. Soc.* **1988**, *110*, 3056−3062. (j) Damrauer, R.; Burggraf, L. W.; Davis, L. P.; Gordon, M. S. *J. Am. Chem. Soc.* **1988**, *110*, 6601−6606. (k) Deiters, J. A.; Holmes, R. R.; Holmes, J. M. *J. Am. Chem. Soc.* **1988**, *110*, 7672−7681. (l) Gronert, S.; Glaser, R.; Streitwieser, A. *J. Am. Chem. Soc.* **1989**, *111*, 3111−3117. (m) Sini, G.; Ohanessian, G.; Hiberty, P. C.; Shaik, S. S. *J. Am. Chem. Soc.* **1990**, *112*, 1407−1413. (n) Fujimoto, H.; Arita, N.; Tamao, K. *Organometallics* **1992**, *11*, 3035−3041.

(8) Theoretical studies concerning pseudorotation processes of pentacoordinate silicon species: (a) Wilhite, D. L.; Spialter, L. *J. Am. Chem. Soc.* **1973**, *95*, 2100−2104. (b) Gordon, M. S.; Windus, T. L.; Burggraf, L. W.; Davis, L. P. *J. Am. Chem. Soc.* **1990**, *112*, 7167−7171. (c) Windus, T. L.; Gordon, M. S.; Burggraf, L. W.; Davis, L. P. *J. Am. Chem. Soc.* **1991**, *113*, 4356−4357.

(9) Review on theoretical studies in organosilicon chemistry: Apeloig, Y. In *The Chemistry of Organic Silicon Compounds*; Patai, S., Rappoport, Z., Eds.; Wiley: Chichester, U.K., 1989; Part 1, pp 57−226.

(10) Tacke, R.; Pikies, J.; Linoh, H.; Rohr-Aehle, R.; Gönne, S. *Liebigs Ann. Chem.* **1987**, 51−57.

Table 1. Crystal Data and Experimental Parameters for the Crystal Structure Analyses of 5, 6, and 7a

	5	6	7a
empirical formula	$C_3H_9F_4NSi$	$C_4H_{11}F_4NSi$	$C_4H_{12}F_3NSi$
formula mass, g mol^{-1}	163.19	177.22	159.23
collection *T*, °C	−110	−110	−100
λ(Mo Kα), Å	0.710 73	0.710 73	0.710 73
cryst syst	triclinic	orthorhombic	monoclinic
space group	$P\bar{1}$	*Pnma*	$P2_1/n$
a, Å	7.449(2)	12.087(3)	5.864(2)
b, Å	8.653(4)	8.364(3)	7.548(2)
c, Å	11.728(5)	7.855(3)	17.038(4)
α, deg	108.08(3)	90	90
β, deg	96.90(3)	90	90.83(2)
γ, deg	101.58(3)	90	90
V, Å^3	690.3(5)	794.1(4)	754.1(3)
Z	2	4	4
D(calcd), g cm^{-3}	1.570	1.482	1.402
μ(Mo Kα), cm^{-1}	3.25	2.88	2.85
F(000)	336	368	336
cryst dimens, mm	0.29 × 0.54 × 0.59	0.43 × 0.47 × 0.56	0.29 × 0.37 × 0.44
2*θ* range, deg	3.0−60.0	3.0−60.0	3.0−55.0
index ranges	$0 \le h \le 10$, $-12 \le k \le 11$, $-16 \le l \le 16$	$0 \le h \le 17$, $0 \le k \le 11$, $0 \le l \le 11$	$-7 \le h \le 0$, $-9 \le k \le 0$, $-22 \le l \le 22$
no. of coll rflns	4115	1419	2052
no. of indep rflns	4064	1276	1742
R_{int}	0.0303		0.0138
no. of rflns used	3396 ($F > 4\sigma(F)$)	795 ($F > 4\sigma(F)$)	1528 ($F > 2\sigma(F)$)
no. of params	236	75	130
abs cor			empirical
S^a	3.73	1.12	2.91
R^b	0.0358	0.0527	0.0305
$R_w{}^c$	0.0309	0.0565	0.0253
max/min res electron dens, e Å^{-3}	+0.31/−0.45	+0.49/−0.80	+0.37/−0.23

[a] $S = \{\sum[w(F_o^2 - F_c^2)^2]/(n-p)\}^{1/2}$: n = no. of reflections; p = no. of parameters. [b] $R = \sum||F_o| - |F_o||/\sum|F_o|$. [c] $R_w = [\sum w(|F_o| - |F_c|)^2/\sum w|F_o|^2]^{1/2}$.

Table 2. Crystal Data and Experimental Parameters for the Crystal Structure Analyses of 7b and 8

	7b	8
empirical formula	$C_4H_{12}F_3NSi$	$C_5H_{14}F_3NSi$
formula mass, g mol^{-1}	159.23	173.25
collection *T*, °C	−100	−100
λ(Mo Kα), Å	0.710 73	0.710 73
cryst syst	monoclinic	monoclinic
space group	$P2_1/c$	$P2_1/c$
a, Å	5.924(2)	7.975(3)
b, Å	16.101(5)	10.720(4)
c, Å	8.621(2)	10.174(4)
α, deg	90	90
β, deg	114.76(3)	103.82(4)
γ, deg	90	90
V, Å^3	746.7(5)	844.6(7)
Z	4	4
D(calcd), g cm^{-3}	1.417	1.363
μ(Mo Kα), cm^{-1}	2.88	2.61
F(000)	336	368
cryst dimens, mm	0.29 × 0.36 × 0.52	0.21 × 0.36 × 0.53
2*θ* range, deg	3.0−60.0	3.0−50.0
index ranges	$0 \le h \le 9$, $0 \le k \le 22$, $-12 \le l \le 12$	$-9 \le h \le 9$, $-12 \le k \le 0$, $0 \le l \le 11$
no. of coll rflns	2447	1584
no. of indep rflns	2182	1489
R_{int}	0.0242	0.0289
no. of rflns used	1730 ($F > 4\sigma(F)$)	1173 ($F > 2\sigma(F)$)
no. of params	131	141
abs cor	empirical	empirical
S^a	3.45	1.53
R^b	0.0425	0.0455
$R_w{}^c$	0.0394	0.0372
max/min res electron dens, e Å^{-3}	+0.38/−0.41	+0.30/−0.30

[a−c] See corresponding footnotes in Table 1.

Table 3. Crystal Data and Experimental Parameters for the Crystal Structure Analyses of 9 and 10

	9	10
empirical formula	$C_{10}H_{21}F_4NSi$	$C_{14}H_{30}F_3NSi$
formula mass, g mol^{-1}	259.36	297.48
collection *T*, °C	−100	−100
λ(Mo Kα), Å	0.710 73	0.710 73
cryst syst	orthorhombic	monoclinic
space group	*Pbca*	*Cc*
a, Å	14.382(3)	19.177(4)
b, Å	11.566(3)	9.650(3)
c, Å	14.815(3)	10.430(2)
α, deg	90	90
β, deg	90	121.73(2)
γ, deg	90	90
V, Å^3	2464.4(10)	1641.5(7)
Z	8	4
D(calcd), g cm^{-3}	1.398	1.204
μ(Mo Kα), cm^{-1}	2.15	1.62
F(000)	1104	648
cryst dimens, mm	0.44 × 0.45 × 0.52	0.34 × 0.42 × 0.56
2*θ* range, deg	3.0−50.0	3.0−55.0
index ranges	$0 \le h \le 17$, $0 \le k \le 13$, $0 \le l \le 17$	$-24 \le h \le 21$, $0 \le k \le 12$, $0 \le l \le 13$
no. of coll rflns	2149	2117
no. of indep rflns	2149	2002
no. of rflns used	1648 ($F > 2\sigma(F)$)	1903 ($F > 2\sigma(F)$)
no. of params	230	279
abs cor		empirical
S^a	2.06	2.06
R^b	0.0487	0.0354
$R_w{}^c$	0.0460	0.0350
max/min res electron dens, e Å^{-3}	+0.35/−0.27	+0.31/−0.30

[a−c] See corresponding footnotes in Table 1.

anions $PhSiF_4^-$ [3b] and $^tBuPhSiF_3^-$,[4d] respectively. The deformation parameters Δ for the tetrafluorosilicates (**5**, 5.9/5.4°; **6**, 3.7°; **9**, 6.0°) are lower than those observed for the trifluorosilicates (**7a**, 9.7°; **7b**, 11.6°; **8**, 8.5°; **10**, 15.1°). The Δ values for the compounds with an N−H

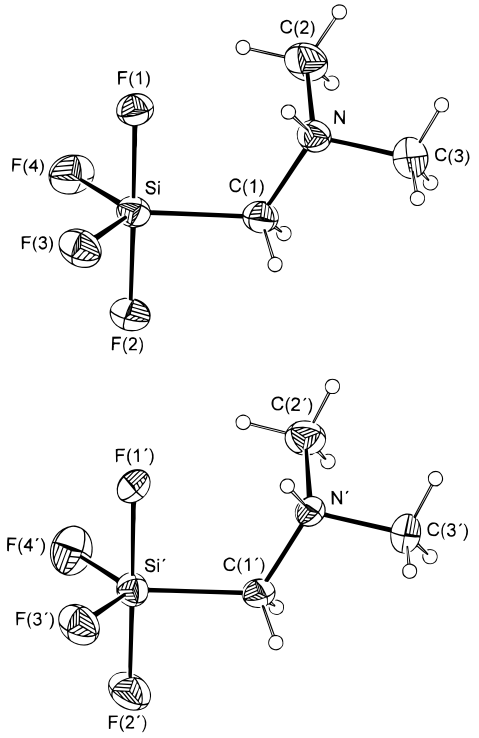

Figure 1. Molecular structures of **5** (above, molecule 1; below, molecule 2) in the crystal state (ORTEP plots, probability levels 50%), showing the atomic numbering scheme.

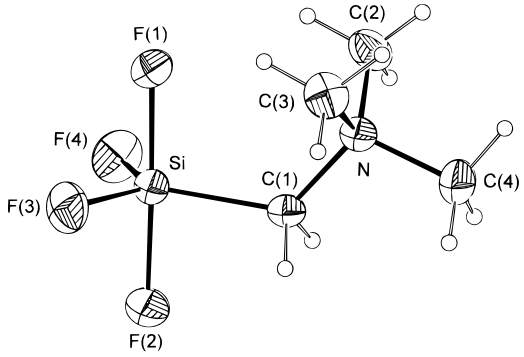

Figure 2. Molecular structure of **6** in the crystal state (ORTEP plot, probability level 50%), showing the atomic numbering scheme. The zwitterion displays crystallographic C_s symmetry: F(3), F(4) and C(2), C(3) are symmetry equivalent.

function (**5**, 5.9/5.4°; **7a**, 9.7°; **7b**, 11.6°) are consistently higher than those found for the corresponding analogues with an NMe moiety instead of the NH group (**6**, 3.7°; **8**, 8.5°).

Except for compounds **8** and **10**, significant differences between the two axial Si−F bond distances of the tri- and tetrafluorosilicates studied are observed (minimum deviation 0.019 Å (**5**, molecule 1); maximum deviation 0.054 Å (**7a**)).

A further remarkable observation concerns the two Si−C bond distances in the trifluorosilicates **7a**,**b** and **8**: in all cases the Si−C(1) distance was found to be significantly shorter than the Si−C(2) distance (differences 0.043 Å (**7a**), 0.046 Å (**7b**), and 0.061 Å (**8**)).

The zwitterionic tri- and tetrafluorosilicates **5**, **7a**,**b**, **9**, and **10**, all with NH groups, display characteristic intramolecular N−H···F hydrogen bonds to their adjacent axial fluorine atoms. Typical N···F and H···F

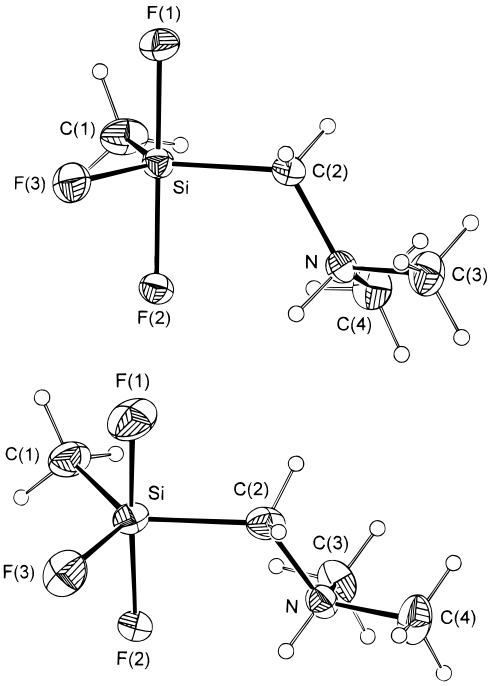

Figure 3. Molecular structures in the crystal state of **7a** (above) and of **7b** (below) (ORTEP plots, probability levels 50%), showing the atomic numbering scheme.

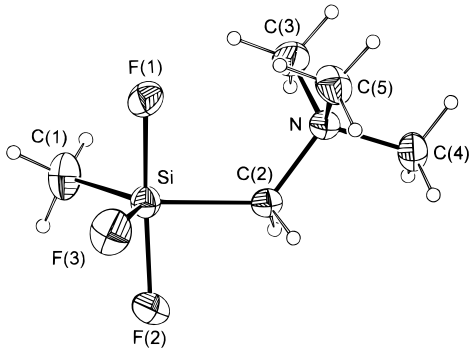

Figure 4. Molecular structure of **8** in the crystal state (ORTEP plot, probability level 50%), showing the atomic numbering scheme.

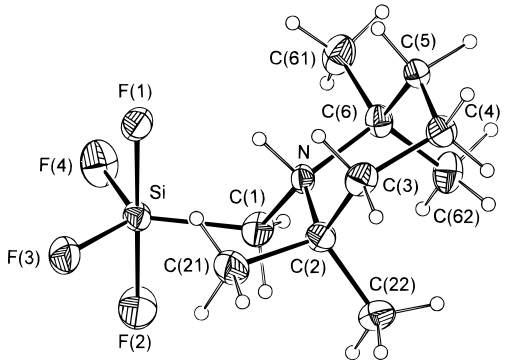

Figure 5. Molecular structure of **9** in the crystal state (ORTEP plot, probability level 50%), showing the atomic numbering scheme.

distances lie in the range of 2.66−2.74 and 1.96−2.33 Å, e.g. values for N···F(2) and H···F(2) of 2.658 and 1.96 Å in **7b**. These intramolecular interactions are augmented in **5** and **7a**,**b** by intermolecular N−H···F interactions to a second zwitterion related by a crystallographic center of symmetry, e.g. distances for N···F(2)′

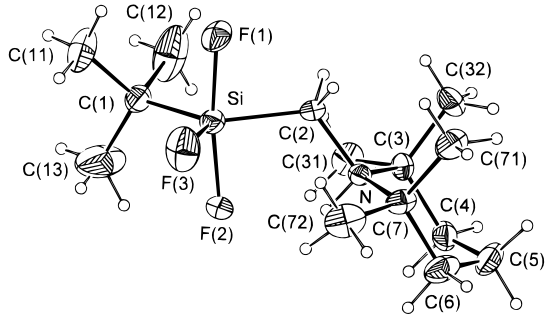

Figure 6. Molecular structure of **10** in the crystal state (ORTEP plot, probability level 50%), showing the atomic numbering scheme.

Table 4. Selected Interatomic Distances (Å) and Angles (deg) for 5[a] and 6

	5 (Molecule 1)	**5** (Molecule 2)	**6**
Si−F(1)	1.690(1)	1.708(2)	1.657(4)
Si−F(2)	1.671(1)	1.664(2)	1.678(4)
Si−F(3)	1.623(2)	1.619(2)	1.607(3)
Si−F(4)	1.606(2)	1.606(1)	1.607(3)
Si−C(1)	1.893(3)	1.888(2)	1.894(6)
F(1)−Si−F(2)	178.34(9)	178.45(9)	178.3(2)
F(1)−Si−F(3)	88.28(7)	87.67(8)	89.6(1)
F(1)−Si−F(4)	90.23(7)	89.43(8)	89.6(1)
F(1)−Si−C(1)	92.52(8)	92.08(8)	96.5(2)
F(2)−Si−F(3)	90.06(8)	90.81(8)	89.5(1)
F(2)−Si−F(4)	90.45(8)	90.99(8)	89.5(1)
F(2)−Si−C(1)	88.4(1)	88.95(9)	85.2(2)
F(3)−Si−F(4)	115.8(1)	116.13(9)	118.0(2)
F(3)−Si−C(1)	121.0(1)	121.19(9)	120.8(1)
F(4)−Si−C(1)	123.2(1)	122.7(1)	120.8(1)
Si−C(1)−N	119.2(2)	118.5(1)	124.8(3)

[a] In this table, the same numbering scheme is used for molecule 1 and molecule 2; the primes for the atoms of molecule 2 (see Figure 1) are omitted for clarity.

Table 5. Selected Interatomic Distances (Å) and Angles (deg) for 7a,b and 8

	7a	**7b**	**8**
Si−F(1)	1.689(1)	1.689(2)	1.694(2)
Si−F(2)	1.743(1)	1.739(1)	1.696(2)
Si−F(3)	1.638(1)	1.629(2)	1.629(2)
Si−C(1)	1.860(2)	1.851(3)	1.856(3)
Si−C(2)	1.903(2)	1.897(2)	1.917(3)
F(1)−Si−F(2)	174.79(6)	174.31(9)	173.6(1)
F(1)−Si−F(3)	89.66(6)	90.36(9)	87.7(1)
F(1)−Si−C(1)	93.75(8)	94.5(1)	92.3(1)
F(1)−Si−C(2)	87.20(7)	86.42(9)	94.1(1)
F(2)−Si−F(3)	86.81(5)	86.97(8)	87.8(1)
F(2)−Si−C(1)	91.31(8)	91.2(1)	93.8(1)
F(2)−Si−C(2)	90.94(7)	90.24(8)	84.1(1)
F(3)−Si−C(1)	119.18(8)	118.0(1)	118.5(1)
F(3)−Si−C(2)	116.31(7)	116.1(1)	119.3(1)
C(1)−Si−C(2)	124.50(9)	125.9(1)	122.1(2)
Si−C(2)−N	118.3(1)	118.6(1)	125.8(2)

and H···F(2)′ for 2.798 and 1.99 Å in **7b**. This means that the NH proton adopts a bifurcating role in these compounds.

NMR Studies at Room Temperature. Compounds **5**−**10** were studied by solution-state ^{1}H, ^{13}C, ^{19}F, and ^{29}Si NMR experiments at room temperature using CD_3CN as solvent (see Experimental Section). For compound **10**, further solvents ($CDCl_3$, CD_2Cl_2, CD_3NO_2) were used in these investigations, leading to results similar to those obtained for CD_3CN. The ^{1}H and ^{13}C NMR data for **5**−**10** are in good accordance with the structures of **5**−**10**. These data reflect the presence of the respective hydrocarbon moieties but do not allow a deeper insight into the molecular structure of these compounds. The ^{19}F NMR spectra of **5**−**10** are characterized by a more or less sharp resonance signal, indicating rapid fluorine exchange at room temperature. All attempts to detect a ^{29}Si resonance signal for **6**−**8** failed. In contrast, for **5**, **9**, and **10** characteristic ^{29}Si NMR spectra could be obtained. The respective ^{29}Si chemical shifts (δ −123.8 (**5**), −123.5 (**9**), −93.6 (**10**)) are typical of pentacoordinate silicon atoms in F_4SiC or F_3SiC_2 frameworks. These data are in good agreement with the isotropic ^{29}Si chemical shifts obtained for **5**, **6**, and **10** in solid-state ^{29}Si CP/MAS experiments (δ −120.6 (**5**), −122.8 (**6**), −97.2 (**10**)). Except for compounds **9** (quint, $^1J_{SiF}$ = 204.4 Hz) and **10** (q, $^1J_{SiF}$ = 261.1 Hz), SiF couplings were not resolved in the ^{29}Si NMR spectra of **5**−**10** in CD_3CN, indicating again a rapid fluorine exchange in solution at room temperature. As shown by temperature-dependent ^{19}F NMR studies of **10** (see next chapter), this ligand exchange can be reduced significantly by cooling.

Table 6. Selected Interatomic Distances (Å) and Angles (deg) for 9

Si−F(1)	1.678(2)	Si−F(4)	1.606(2)
Si−F(2)	1.649(2)	Si−C(1)	1.888(4)
Si−F(3)	1.601(3)		
F(1)−Si−F(2)	179.7(1)	F(2)−Si−C(1)	88.5(2)
F(1)−Si−F(3)	89.6(1)	F(3)−Si−F(4)	114.3(1)
F(1)−Si−F(4)	88.9(1)	F(3)−Si−C(1)	124.4(1)
F(1)−Si−C(1)	91.2(2)	F(4)−Si−C(1)	121.3(2)
F(2)−Si−F(3)	90.6(1)	Si−C(1)−N	119.7(2)
F(2)−Si−F(4)	91.3(1)		

Table 7. Selected Interatomic Distances (Å) and Angles (deg) for 10

Si−F(1)	1.707(2)	Si−C(1)	1.914(4)
Si−F(2)	1.709(2)	Si−C(2)	1.918(3)
Si−F(3)	1.624(2)		
F(1)−Si−F(2)	172.4(1)	F(2)−Si−C(2)	89.0(1)
F(1)−Si−F(3)	90.7(1)	F(3)−Si−C(1)	113.9(1)
F(1)−Si−C(1)	92.8(1)	F(3)−Si−C(2)	118.5(1)
F(1)−Si−C(2)	83.9(1)	C(1)−Si−C(2)	127.5(1)
F(2)−Si−F(3)	90.5(1)	Si−C(2)−N	120.6(2)
F(2)−Si−C(1)	93.6(1)		

Temperature-Dependent ^{19}F NMR Studies of 10. The low-temperature (−90 °C) ^{1}H and ^{19}F NMR spectra of the trifluorosilicate **10** (Figure 7) confirm the structure determined by X-ray analysis. The ^{19}F NMR spectrum shows three signals at δ −98.5 (triplet), −105.9 (doublet), and −145.9 (singlet) of relative intensities 1:1:1. The fine structure of the low-field signal results from couplings with two different spin $^1/_2$ nuclei having nearly identical coupling constants. One of the coupling partners is the fluorine nucleus showing a doublet at δ −105.9 ($^2J_{FF}$ = 35 Hz). Since the third fluorine signal does not show any fine structure, the second coupling partner must be a proton. Decoupling experiments indeed confirmed that the ammonium proton shows a fluorine coupling of 31 Hz. In the ^{1}H NMR spectrum, the ammonium proton causes a broad doublet at δ −6.2 which collapses into a singlet on selective decoupling of the fluorine signal at δ −98.5 (see Figure 7). Considering the value of the coupling constant of 31 Hz, a through-space H,F coupling rather than a through-bond ^4J(H,F) coupling has to be assumed. Even for this type of interaction the value is quite large but still falls into the upper range of other through-space H,F couplings described in the literature

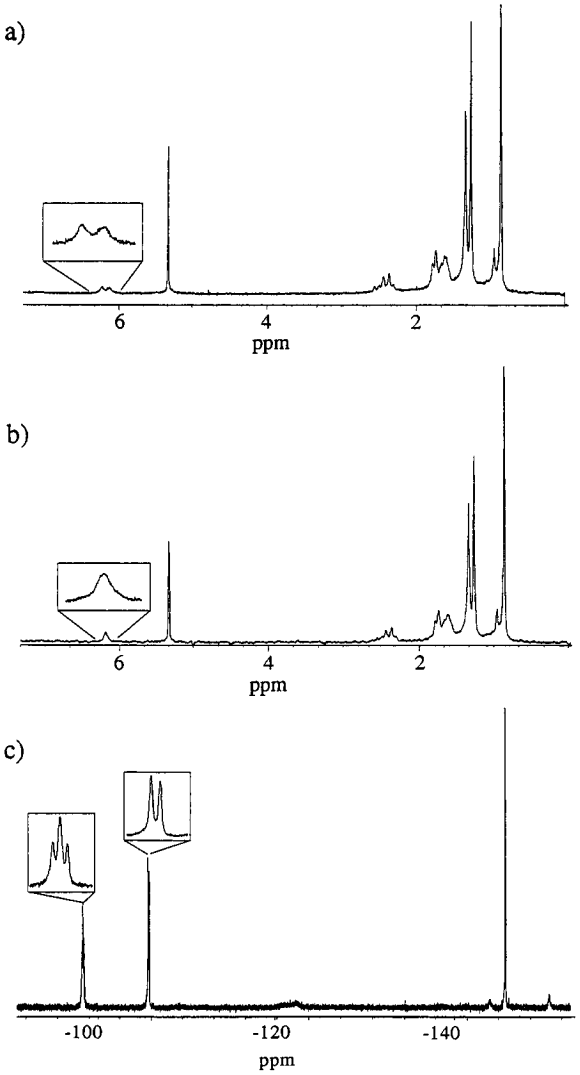

Figure 7. (a) ^{1}H NMR spectrum (300.1 MHz), (b) ^{19}F-decoupled ^{1}H NMR spectrum (300.1 MHz), and (c) ^{19}F NMR spectrum (282.4 MHz) of **10** in CD_2Cl_2 at −90 °C.

(in this context, see ref 11). Furthermore, the H−F distance of 2.05 Å (calculated from the atomic coordinates) between the ammonium proton and the neighboring axial fluorine atom is indicative of outer orbital interactions of these two nuclei. From these considerations, the low-field triplet must be assigned to the axial fluorine atom close to the ammonium proton. Since $^{2}J_{F_{ax}F_{ax}}$ is known to be larger than $^{2}J_{F_{ax}F_{eq}}$, the doublet at δ −105.9 and the singlet at δ −145.9 can be assigned to the second fluorine atom in the axial position and to the equatorial fluorine atom, respectively.

When the temperature increases, the signals of the two axial fluorine atoms are broadened (see Figure 8). Line broadening also appears for the doublet of the ammonium proton. All other lines in the ^{1}H NMR spectrum remain unaffected within the whole temperature range up to 33 °C; thus, reversal of the chair conformation of the piperidinio ring can be excluded. Reversal of the ring conformation is probably hindered by the bulky $CH_2Si^tBuF_3$ group, preferring the equatorial position. Since the two signals of the axial fluorine atoms show coalescence at −23 °C, the dynamic process observed must be an exchange between these two nuclei.

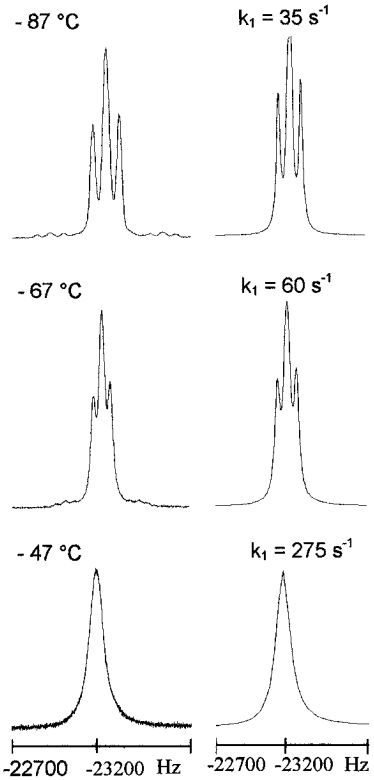

Figure 8. Temperature-dependent experimental (left) and simulated (right) ^{19}F NMR spectra of **10** (low-field signal, frequency range −22 700 to −23 700 Hz). For the experimental conditions, see Experimental Section. For the calculations, F,F and H,F couplings were taken into account.

Site exchange between the axial fluorine atoms can only be caused by rotation of the (piperidinio)methyl group around the Si−C bond.

In the temperature range between −87 and −47 °C, the line shape of the ^{19}F NMR spectra was calculated on the basis of a four-spin system undergoing exchange between two sites (ABMX ⇌ BAMX), using the computer program DNMR5 (see Figure 8).[12] The four spins are given in the order F_{ax} (J_{HF} = 31 Hz), F_{ax} (J_{HF} = 0 Hz), F_{eq}, and H.

A second exchange process is indicated by line broadening of the high-field signal in the ^{19}F NMR spectrum above −47 °C (Figure 9). This process leads to coalescence of all three fluorine signals at 20 °C. The equilibrium of the fluorine atoms is assumed to be caused by a pseudorotation-like process at the silicon atom as discussed in Intramolecular Ligand Exchange.

The mixed process of the rotation of the (piperidinio)-methyl group around the Si−C bond and the "pseudorotation" causes an exchange of the given four-spin system ABMX between six different sites. This, however, exceeds the capabilities of the program we presently use. The effect of both processes on the line shape was therefore calculated by a simple approximation omitting the effect of F,F coupling (see Figure 9). Since the chemical shifts are larger than the coupling constant by a factor of 350, this approximation does not lead to significant errors. Calculations for the simple Si−C rotation process using the same approximation resulted

(11) Fritz, H.; Winkler, T. *Helv. Chim. Acta* **1974**, *57*, 836−839.

(12) Stephenson, D. S.; Binsch, G. *QCPE* **1978**, *No. 365*.

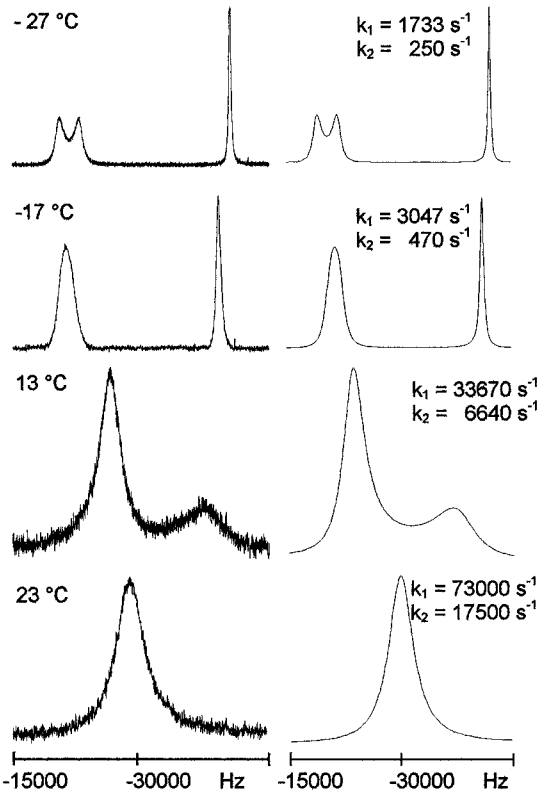

Figure 9. Temperature-dependent experimental (left) and simulated (right) ^{19}F NMR spectra of **10** (frequency range −15 000 to −45 000 Hz). For the experimental conditions, see Experimental Section. For the calculations, only H,F coupling was taken into account.

in rate constants differing by about 15 s^{-1} compared to those of the correct description. This may lead to a systematic deviation of $\Delta S^{\ddagger}$ of about 1 J mol^{-1} K^{-1}. At temperatures above the coalescence temperature of the two low-field signals the rate constants k_1 for the Si−C rotation can no longer be exactly determined from the line shape. This also influences the accuracy of k_2. In order to get reliable rate constants k_2 for the pseudorotation, k_1 values obtained at lower temperatures were extrapolated to the high-temperature range, where they were used as constant input data.

The rate constants k_1 and k_2 obtained from the line shape analyses (see Figures 8 and 9) were fitted to the Eyring equation in order to get the activation parameters for the two dynamic processes. For the Si−C rotation, the values $\Delta H^{\ddagger} = 40.9 \pm 1.2$ kJ mol^{-1} and $\Delta S^{\ddagger} = -15.4 \pm 0.6$ J mol^{-1} K^{-1} were calculated. The activation parameters for the pseudorotation process were found to be $\Delta H^{\ddagger} = 44.4 \pm 1.6$ kJ mol^{-1} and $\Delta S^{\ddagger} = -16.5 \pm 0.7$ J mol^{-1} K^{-1}. The high negative value of $\Delta S^{\ddagger}$ for the pseudorotation process is a consequence of the presumption that the transmission coefficient κ is set to 1. As may be gathered from Figures 20 and 21, the ligand exchange process of **10** also should involve more than one transition state, leading to a κ value less than 1. Assuming that three intermediates are involved (e.g. **20b**,**d**,**e**; see Figure 21), a decrease of the transmission coefficient by a factor of $^1/_2$ for each intermediate results in a $\Delta S^{\ddagger}$ value of 1.9 J mol^{-1} K^{-1}.

Theoretical Studies: General and Methodical Aspects. The structure and dynamic behavior of the title compounds were studied by quantum-chemical methods. For this purpose, geometry optimizations at the SCF[13] (self-consistent field) and MP2[14] (Møller−Plesset perturbation theory) level of some of these compounds and related model species were performed using the TURBOMOLE[15] program system. Stationary geometries and transition states were characterized as local minima and saddle points, respectively, by calculation of the vibrational frequencies. Unless denoted otherwise, all energies given include the single-point MP2 energy and the zero vibrational energy. The basis sets employed are given in Table 8.

Table 8. Basis Sets (EXT, TZP, SVP) Used for the Theoretical Studies

EXT	Si	(13s10p2d1f)/[8s6p2d1f]	
	F, O, N, C	(13s8p2d1f)/[8s5p2d1f]	
	H	(6s2p1d)/[3s2p1d]	
TZP	Si	(12s9p1d)/[7s5p1d]	$\eta_d = 0.60$
	F, O, N, C	(10s6p1d)/[6s3p1d]	$\eta_d = 0.62/0.71/0.92/0.80$
	H	(5s1p)/[3s1p]	$\eta_p = 1.00$
SVP	Si	(10s7p1d)/[4s3p1d]	
	F, O, N, C	(7s4p1d)/[3s2p1d]	
	H	(4s)/[2s]	

The EXT basis set (extended basis set) was used as a reference for the SCF calculations to ascertain the accuracy of the smaller SVP (split valence polarization) basis set used in these studies. The EXT basis set was taken from ref 16, and a large polarization basis (2d1f for Si, F, O, N, and C; 2p1d for H) taken from ref 17 was added. The TZP (triple-ζ polarization) basis set was used for the MP2 calculations, which served as a reference to ascertain the accuracy of the more approximate treatments. The TZP basis was derived from the atomic TZ basis,[16] and the orbital exponents of the polarization functions for Si, F, O, and N were taken from the optimized d functions of the SVP basis.

The SVP basis set given in ref 16 is suitable to describe molecules with moderately polarized chemical bonds. Therefore, we additionally optimized the exponents of the most diffuse s, p, and d GTOs (Gauss type orbitals) for Si, F, O, and N at the SCF level to get a more accurate description of pentacoordinate silicon species containing distinctly polarized silicon−element bonds. For this purpose, an SVP basis set optimization was performed for the model molecule (ammoniomethyl)[1,2-ethenediolato(2−)]difluorosilicate (**18**).[18] The

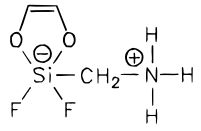

18

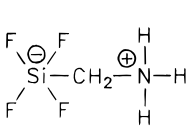

19

most conspicuous changes concern the d functions, which were significantly flattened by this optimization for F and O but were contracted for Si (see Table 9).

(13) Roothaan, C. C. J. *Rev. Mod. Phys.* **1951**, *23*, 69−89.
(14) Møller, C.; Plesset, M. S. *Phys. Rev.* **1934**, *46*, 618−622.
(15) Ahlrichs, R.; Bär, M.; Häser, M.; Horn, H.; Kömel, C. *Chem. Phys. Lett.* **1989**, *162*, 165−169.
(16) Schäfer, A.; Horn, H.; Ahlrichs, R. *J. Chem. Phys.* **1992**, *97*, 2571−2577.
(17) Huzinaga, S. *Gaussian Basis Sets for Molecular Calculations*; Elsevier: Amsterdam, 1974.
(18) This particular molecule with an SiO_2F_2C framework was chosen because it also shall serve as a model for theoretical studies of related λ^5*Si*-silicates containing bidentate *vic*-diolato(2−) ligands (e.g. 1,2-benzenediolato(2−) ligands). Compounds of this formula type are currently under investigation: Dannappel, O.; Tacke, R. Unpublished results.

Table 9. Comparison of Standard Exponents and Optimized Exponents of the SVP Basis (Si, F, O, and N) Used

atom	function	SVP[16]	SVP_{opt}[a]
Si	η_{s9}	0.205	0.255
	η_{s10}	0.078	0.058
	η_{p7}	0.100	0.081
	η_{d}	0.350	0.600
F	η_{s7}	0.332	0.323
	η_{p4}	0.348	0.351
	η_{d}	1.400	0.620
O	η_{s7}	0.255	0.260
	η_{p4}	0.276	0.280
	η_{d}	1.200	0.707
N	η_{s7}	0.188	0.352
	η_{p4}	0.220	0.253
	η_{d}	1.000	0.920

[a] For the symmetrically independent fluorine and oxygen atoms of the model species **18**, the average was taken.

Table 10. Calculated Interatomic Distances (Å), Angles (deg), and Energies (hartree) for 19 (C_s Symmetry) at Various Levels of Theory[a]

	SCF/ SVP[16]	SCF/ SVP_{opt}	SCF/ EXT	MP2/ TZP
Si−F(1)	1.703	1.686	1.689	1.731
Si−F(2)	1.653	1.635	1.638	1.667
Si−F(3/4)	1.613	1.592	1.589	1.621
Si−C	1.941	1.939	1.941	1.933
C−N	1.513	1.512	1.515	1.512
C−H(1/2)	1.090	1.090	1.080	1.087
N−H(3/4)	1.013	1.015	1.004	1.021
N−H(5)	1.012	1.014	1.003	1.019
F(1)−Si−F(2)	173.5	172.6	173.0	172.7
F(1)−Si−F(3/4)	90.2	90.5	90.4	90.1
F(1)−Si−C	87.1	86.6	87.2	86.7
F(2)−Si−F(3/4)	93.0	93.3	93.1	93.5
F(2)−Si−C	86.4	86.0	85.9	86.1
F(3)−Si−F(4)	121.1	119.6	120.1	120.5
F(3/4)−Si−C	119.4	120.2	119.9	119.7
energy	−781.61554	−781.65420	−782.39641	−782.34654

[a] For the atomic numbering scheme, see Figure 9.

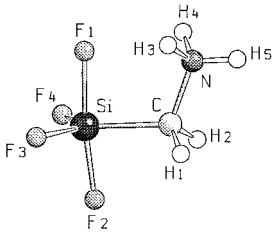

Figure 10. Calculated structure of **19** (C_s symmetry), showing the atomic numbering scheme (for the geometric data, see Table 10).

The SCF energy of **18** was improved by 79.8 kJ mol^{-1} when the optimized SVP basis set was used.[19]

To get an idea about the accuracy of the calculations performed in this study, geometry optimizations at various levels of theory (SCF/SVP, SCF/EXT, MP2/TZP) were carried out for the model molecule (ammoniomethyl)tetrafluorosilicate (**19**; C atom in an equatorial position). The bond distances and angles and the energies obtained in these calculations are compared in Table 10; the calculated structure of **19** is depicted in Figure 10.

The data obtained with the optimized SVP basis set were very similar to those calculated with the SCF/EXT basis. The bond distances of the silicon−element bonds differ only by maximally 0.003 Å and the bond angles by maximally 0.6°. When using the nonoptimized SVP basis set, larger differences were observed. The Si−F bond distances obtained in the MP2/TZP calculations were found to be somewhat longer (0.029−0.045 Å) than those obtained in the SCF/SVP (optimized basis set) calculations, whereas the Si−C bond was found to be shorter by 0.006 Å. The dihedral angles around the silicon atom are only slightly affected by maximally 0.9°. This result is further confirmed by the respective data obtained in SCF/SVP (optimized basis set) and MP2/TZP calculations for several local minima of the zwitterion (ammoniomethyl)trifluoro(methyl)silicate (**20**) (see Intramolecular Ligand Exchange). In conclusion, these results demonstrate that the SCF/SVP treatment with the optimized basis set is of sufficient reliability for the theoretical description of the title compounds.

Table 11. Selected Mulliken Brutto Populations ρ, Overlap Populations, and Force Constants (N m^{-1}) for 19

atom	brutto population	overlap population (Si−X bond)	force constant (Si−X bond)
Si	2.31		
F(1)	−0.70	0.35	382
F(2)	−0.66	0.42	503
F(3/4)	−0.62	0.51	625
C	−0.72	0.33	306

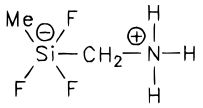

20

Description of the Chemical Bond. The concept of a three-center−four-electron bond (combination of a doubly occupied bonding MO and a nonbonding MO) for the description of the orbital interactions around the pentacoordinate silicon atom of anionic λ^5Si species seems to be favored.[6] This model can also be used for the qualitative characterization of the zwitterionic λ^5*Si*-silicate **19**; however, for a more detailed description of the strongly polarized Si−F and Si−C bonds in this molecule, a modification of the bond model is required. A Mulliken population analysis[20] and force constant calculations for **19** (C atom in an equatorial position) clearly indicate that the bond order of the axial and equatorial bonds does not differ as much as would be expected for a three-center−four-electron model (see Table 11). The Mulliken population analysis leads to the following orbital occupations for the silicon atom: 0.41 (3s), 0.36 ($3p_x$), 0.31 ($3p_y$), 0.30 ($3p_z$), and 0.30 (total 3d population). This shows that the stabilizing influence of the 3s orbitals is slightly greater than that of the 3p AOs and that the 3d AOs contribute significantly less to bonding. Although a negative charge is formally assigned to the pentacoordinate silicon atom of **19**, it represents an electrophilic center, the negative charge being mainly localized on the fluorine atoms.

The calculated energy for the dissociation of **19** according to the reaction $F_4SiCH_2NH_3 \rightarrow F_3SiCH_2NH_2$

(19) Calculated SCF energies (hartree) for **18**: SVP,[16] −809.270 13; SVP_{opt}, −809.300 54.

(20) Mulliken, R. *J. Chem. Phys.* **1955**, *23*, 1833−1837.

Table 12. Selected Calculated Interatomic Distances (Å) and Angles (deg) for 5 and 7 and Differences from the Respective Data Obtained by X-ray Diffraction Studies

	5	Δ to X-ray data[a]	7	Δ to X-ray data[b]
Si−F(1)	1.696	−0.003	1.657	−0.032
Si−F(2)	1.634	−0.034	1.729	−0.012
Si−F(3)	1.596	−0.025	1.605	−0.029
Si−[F(4)/C(2)]	1.593	−0.013	1.953	0.053
Si−C(1)	1.938	0.047	1.873	0.017
F(1)−Si−F(2)	173.9	−4.5	170.9	−3.7
F(1)−Si−F(3)	89.3	1.3	92.5	2.5
F(1)−Si−[F(4)/C(2)]	90.3	0.5	85.0	−2.2
F(1)−Si−C(1)	86.9	−5.4	94.1	0.0
F(2)−Si−F(3)	92.4	2.0	89.0	2.2
F(2)−Si−[F(4)/C(2)]	93.9	3.2	86.2	−4.7
F(2)−Si−C(1)	87.2	−1.5	92.9	1.6
F(3)−Si−[F(4)/C(2)]	120.0	4.0	115.8	−0.5
F(3)−Si−C(1)	122.4	1.3	120.4	1.2
[F(4)/C(2)]−Si−C(1)	117.5	−5.5	123.8	−0.7

[a] For calculation of these differences, the average of the corresponding data of the two crystallographically independent molecules was taken. [b] For calculation of these differences, the average of the corresponding data of the two crystallographic modifications (**7a**,**b**) was taken.

+ HF (ΔE_{calc} = 23.6 kJ mol^{-1})[21] is quite moderate. Thus, the thermodynamic stability of the zwitterionic λ^5*Si*-silicate **19** is only somewhat greater than that of the system $F_3SiCH_2NH_2$/HF, and therefore, **19** might act as an HF donor.

Comparison of Calculated and Experimental Geometric Data. SCF/SVP geometry optimizations for the zwitterionic λ^5*Si*-silicates **1**, **3**, and **5**−**7** were performed and the resulting geometric data compared with those obtained experimentally by single-crystal X-ray diffraction studies.[22] As an example of these investigations, selected calculated and experimental bond distances and angles for **5** and **7** are compared in Table 12; the calculated structures of **5** and **7** are depicted in Figure 11.

For all calculated structures similar trends were observed. By analogy to the experimental results, the coordination polyhedra around the silicon atoms can be best described as a slightly distorted TBP, the axial positions being occupied by fluorine atoms. The calculated bond distances of the two axial Si−F bonds differ by 0.03−0.06 Å, and in all cases the longer distance was found for that Si−F moiety whose F···N distance is shorter. We suggest that dipolar interactions of the type F_{ax}···H−N or F_{ax}···Me−N may be responsible for this weakening of the Si−F_{ax} bond. For example, in the case of the zwitterion **7** there are strong indications for such an intramolecular F(2)···H−N interaction (F(2)···H = 1.795 Å; F(2)···N = 2.505 Å; F(2)···H−N = 123.6°; F···H Mulliken overlap population 0.06). In contrast to these consistent results, in the crystal structures of **1**, **3**, and **5**−**7** no systematic lengthening of this kind was observed for one of the two Si−F_{ax} distances, indicating the presence of intermolecular interactions in the crystal that affect the Si−F_{ax} bond distances. Generally, the calculated Si−F_{ax} and Si−F_{eq} bond distances were found to be shorter by 0.01−0.03 Å than those established experimentally, as would be expected when neglecting effects of electron correlation. A good agreement between calculated and experimental data was also observed for the Si−C_{Me} bond distances (maximum deviation 0.015 Å).

In contrast to the above-mentioned good agreement, a comparison of the calculated and experimental data for the Si−C_{CH_2} bond distance revealed unexpected differences, the calculated distances being longer by 0.03−0.055 Å. As effects of electron correlation should shorten the Si−C bond by only 0.01 Å, another explanation for this lengthening is necessary.

The calculated Si−C_{CH_2} bond distances are indeed significantly longer as compared to those of "normal" Si−C bonds.[23] In order to explain this phenomenon, geometry optimizations (C_s symmetry; C atom in an equatorial position) for the zwitterionic λ^5*Si*-silicates **19** and **21**−**25** and the corresponding isoelectronic anionic λ^5*Si*-silicates **26**−**32** were performed[24] and the resulting data compared. Selected bond distances and angles

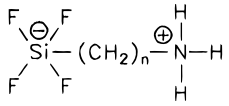

21-25

	21	22	23	24	25
n	2	3	4	5	6

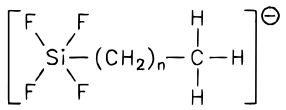

26-32

	26	27	28	29	30	31	32
n	0	1	2	3	4	5	6

obtained in these calculations are given in Table 13 (zwitterions **19** and **21**−**25**) and Table 14 (anions **26**−**32**). As examples of these series of isoelectronic zwitterions and anions, the calculated structures of **23** and **30** are depicted in Figure 12. The atomic numbering scheme shown in this figure was also used for the other species studied.

For the geometric data of the isoelectronic zwitterions and anions quite different trends were observed, indicating the significant influence of the ammonio group on the Si−C distance. In the case of the zwitterions, lengthening of the alkylene chain leads to a gradual shortening of the Si−C distance and to a decrease of the difference between the Si−F_{ax} distances. The Si−C bond of the anions, however, does not show an unusual lengthening, and the Si−C distance does not signifi-

(21) Geometries were optimized at the SCF/TZP level (SCF + single point MP2 + E_{vib0} energies (hartree): **19**, −783.734 53; $F_3SiCH_2NH_2$, −683.433 81; HF, −100.291 73).

(22) According to the experimentally established Si coordination polyhedra, only minima with carbon atoms in equatorial positions were treated. Calculated SCF energies (hartree) (C_1 symmetry for **1**, **3**, **5**, and **7**; C_s symmetry for **6**): **1**, −936.531 76; **3**, −876.675 56; **5**, −859.658 06; **6**, −898.670 53; **7**, −799.801 31.

(23) Lukevics, E.; Pudova, O.; Sturkovich, R. *Molecular Structure of Organosilicon Compounds*; Wiley: Chichester, U.K., 1989; pp 11−18.

(24) Calculated SCF energies (hartree) (C_s symmetry; C atom in an equatorial position): **21**, −820.623 14; **22**, −859.602 14; **23**, −898.586 52; **24**, −937.576 37; **25**, −976.568 20; **26**, −726.157 13; **27**, −765.157 73; **28**, −804.160 60; **29**, −843.162 79; **30**, −882.164 70; **31**, −921.166 53; **32**, −960.168 30.

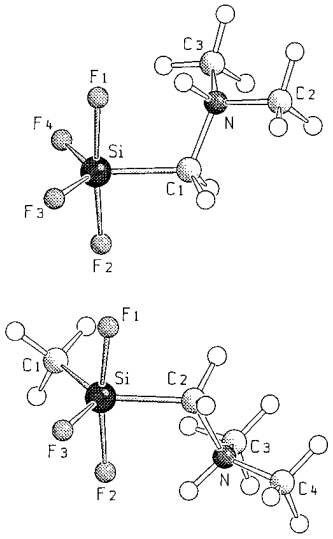

Figure 11. Calculated structures of **5** (C_1 symmetry; above) and **7** (C_1 symmetry; below), showing the atomic numbering scheme.

Table 13. Selected Calculated Interatomic Distances (Å) and Angles (deg) for 19 and 21−25

	19	21	22	23	24	25
Si−F(1)	1.686	1.662	1.664	1.661	1.662	1.661
Si−F(2)	1.635	1.632	1.638	1.644	1.646	1.649
Si−F(3/4)	1.592	1.581	1.588	1.591	1.594	1.596
Si−C(1)	1.939	1.929	1.924	1.918	1.914	1.912
F(1)−Si−F(2)	172.6	174.7	177.3	178.3	179.3	179.7
F(1)−Si−F(3/4)	90.5	90.3	89.7	89.7	89.5	89.5
F(1)−Si−C(1)	86.6	88.0	89.8	90.5	91.1	91.4
F(2)−Si−F(3/4)	93.0	91.5	90.8	90.3	90.1	89.8
F(2)−Si−C(1)	86.0	86.7	87.5	87.8	88.2	88.3
F(3)−Si−F(4)	119.6	118.8	118.8	118.4	118.2	118.0
F(3)−Si−C(1)	120.2	120.6	120.6	120.8	120.9	121.0

Table 14. Selected Calculated Interatomic Distances (Å) and Angles (deg) for 26−32

	26	27	28	29	30	31	32
Si−F(1)	1.652	1.657	1.657	1.657	1.657	1.658	1.658
Si−F(2)	1.658	1.657	1.657	1.657	1.657	1.656	1.657
Si−F(3/4)	1.603	1.602	1.602	1.601	1.601	1.601	1.601
Si−C(1)	1.899	1.907	1.907	1.907	1.907	1.907	1.908
F(1)−Si−F(2)	178.7	178.7	178.8	178.7	178.7	178.8	178.8
F(1)−Si−F(3/4)	89.8	89.3	89.3	89.3	89.3	89.3	89.3
F(1)−Si−C(1)	91.9	92.5	92.5	92.6	92.6	92.5	92.5
F(2)−Si−C(3/4)	88.9	89.1	89.1	89.1	89.2	89.2	89.2
F(2)−Si−C(1)	89.4	88.8	88.7	88.7	88.7	88.7	88.7
F(3)−Si−F(4)	116.8	117.0	117.0	117.0	117.0	117.0	117.0
F(3)−Si−C(1)	121.6	121.5	121.5	121.5	121.5	121.5	121.5

cantly depend on the length of the alkyl group. Furthermore, the Si−F_{ax} distances of the anions are quite similar and also do not depend on the length of the alkyl group.

These results are confirmed by the charge distributions in the zwitterions **19** and **21**−**25** and the anions **26**−**32**, as shown by Mulliken population analyses. When the zwitterions and anions along the alkylene chain were split into SiF_4, CH_2, and NH_3/CH_3 fragments and the respective Mulliken brutto populations of these moieties were observed, quite different trends were noted for the zwitterions and anions (see Figures 13 and 14). In the anionic species **26**−**32**, the negative charge is mainly localized on the F_4SiCH_2 fragment and the charge distribution does not depend on the length of the alkyl group. Thus, the coordination polyhedron around the silicon atom is not significantly influenced by the

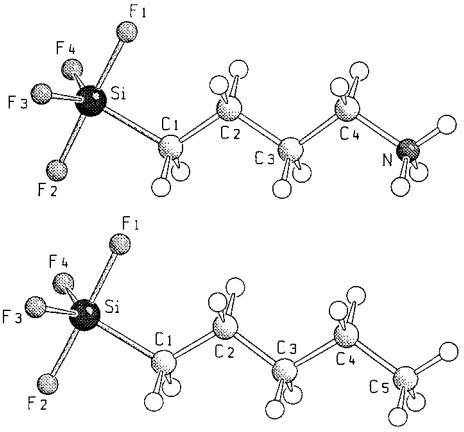

Figure 12. Calculated structures of the isoelectronic species **23** (C_s symmetry; above) and **30** (C_s symmetry; below), showing the atomic numbering schemes. For **19**, **21**, **22**, **24**−**29**, **31**, and **32** an analogous atomic numbering scheme was used.

nature of the alkyl group. In the zwitterions **19** and **21**−**25**, the negative charge is also mainly localized on the SiF_4CH_2 fragment, and the positive charge is mainly found on the CH_2NH_3 moiety. In the molecules **19**, **21**, and **22**, the negative and positive charges are close together and cannot be sufficiently separated. In the case of longer chain lengths (**23**−**25**), however, a clearer charge separation and an almost constant charge distribution along the alkylene fragment is found. All these trends correlate with the calculated bond distances of the zwitterions **19** and **21**−**25** and the anions **26**−**32**.

Geometry optimizations for the model species (aminomethyl)tetrafluorosilicate (**33**) and bis(ammoniomethyl)trifluorosilicate (**34**)[25] additionally demonstrate that an ammonio moiety close to the silicon atom is responsible for the significant lengthening of the Si−C distance. For

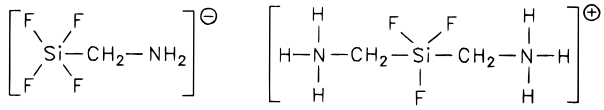

33 **34**

the anion **33** (a derivative of the zwitterion **19** and the anion **27**) a rather "normal" Si−C distance of 1.909 Å was calculated, indicating that the presence of a nitrogen atom close to the silicon atom is not sufficient for lengthening of the Si−C distance; rather, the presence of an ammonio moiety is required. On the other hand, for the cation **34** (a derivative of the zwitterion **7**) significantly lengthened Si−C bond distances of 1.931 Å were found, as would be expected for such a species containing two ammonio groups close to the silicon atom.

In order to explain the discrepancies concerning the calculated and experimental Si−C_{CH_2} bond distances for **1**, **3**, and **5**−**7**, further ab initio studies were performed. A likely explanation of these differences in shortening of the Si−C_{CH_2} bond in the crystal is that they are the result of electrostatic interactions with neighboring molecules which may influence the charge distribution

(25) Calculated SCF energies (hartree) (C atoms in equatorial positions): **33**, −781.131 79 (C_s symmetry); **34**, −777.170 53 (C_2 symmetry).

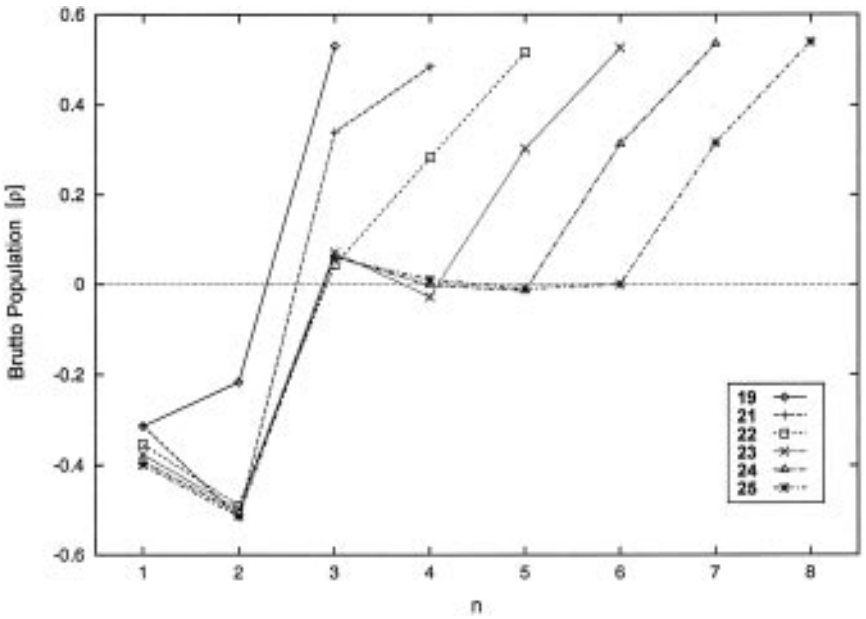

Figure 13. Calculated charge distribution in the zwitterionic silicates **19** and **21**−**25**. Identical symbols are assigned to all fragments of one particular molecule; neighboring fragments of this molecule are connected by lines. The fragments are SiF_4 ($n = 1$), NH_3 (n_{max}), and CH_2 ($1 < n < n_{max}$).

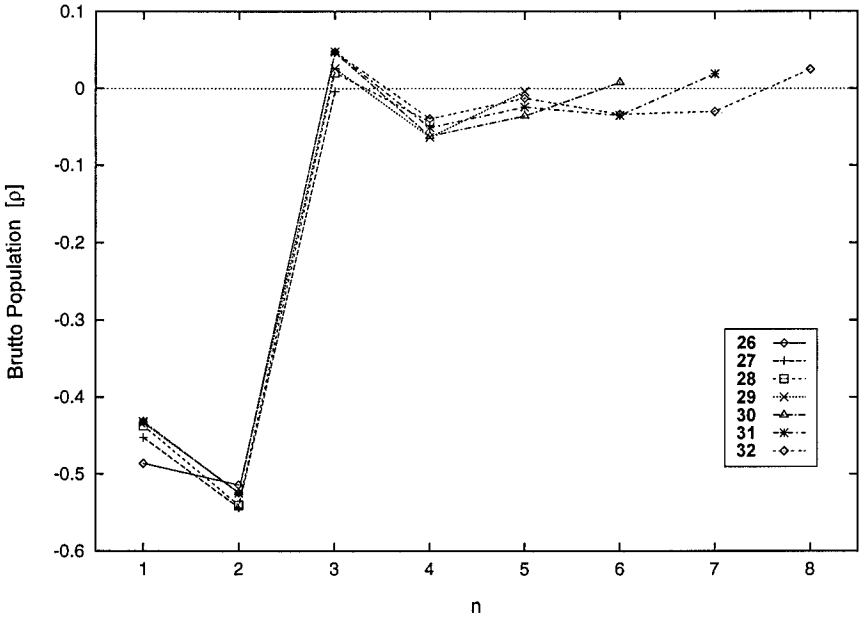

Figure 14. Calculated charge distribution in the anionic silicates **26**−**32**. Identical symbols are assigned to all fragments of one particular ion; neighboring fragments of this ion are connected by lines. The fragments are SiF_4 ($n = 1$), CH_3 (n_{max}), and CH_2 ($1 < n < n_{max}$).

of the zwitterions and especially affect the bonds along the molecular dipole (in this context, see ref 26). This hypothesis is additionally supported by the results of geometry optimizations for the zwitterion **19** in the presence of dummy charges[27] close to its cationic and anionic center. These dummy charges were used to simulate an electrostatic field around this zwitterion in order to get closer to the situation of this molecule in the crystal. As a result of this, shortening of the Si−C distance from 1.939 to 1.910 Å was observed.

Similar results were obtained from ab initio studies of the dimeric zwitterion **19** (see Figure 15).[28] The geometry optimization revealed a considerable dimerization energy of −186.0 kJ mol^{-1}, the monomeric moieties being connected by intermolecular N−H···F(1′) hydrogen bonds (N−H = 1.022 Å; H···F(1′) = 1.735 Å; N···F(1′) = 2.745 Å; N−H···F(1′) = 169.2°; Mulliken overlap population for the H···F(1′) moiety 0.055). In comparison to monomeric **19**, the Si−F(1) distance of

(26) An analysis of the electron density in **1**, **3**, and **5**−**7** reveals dipole moments of 10.5−12.5 D. An analogous effect on a bond along the dipole vector caused by solvation or crystal packing has already been reported for $H_3B{-}NH_3$. In this zwitterion, the B−N distance observed by X-ray diffraction studies is about 0.1 Å shorter than that found by ab initio studies and microwave spectroscopy. (a) Haarland, A. *Angew. Chem.* **1989**, *101*, 1017−1032; *Angew. Chem., Int. Ed. Engl.* **1989**, *28*, 992−1008. (b) Bühl, M.; Steinke, T.; Schleyer, P. v. R.; Boese, R. *Angew. Chem.* **1991**, *103*, 1179−1181; *Angew. Chem., Int. Ed. Engl.* **1991**, *30*, 1160−1162.

(27) Charges of +0.5 e fixed at a distance of 2.91 Å to each fluorine atom on the extended Si−F bond vectors; charges of −0.66 e fixed at a distance of 2.75 Å to each ammonio-hydrogen atom on the extended N−H bond vectors. Calculated SCF energy (hartree): $\mathbf{19}_{dummy}$, −781.852 40 (C_s symmetry). Selected interatomic distances (Å): Si−F(1), 1.674; Si−F(2), 1.655; Si−F(3/4), 1.616; Si−C, 1.910.

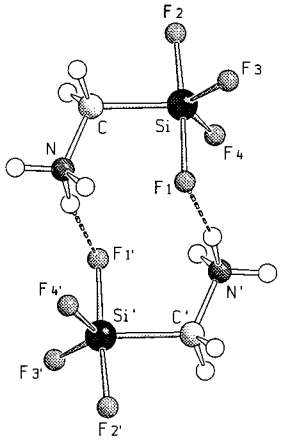

Figure 15. Calculated structure of the dimer of **19** (C_i symmetry), showing the atomic numbering scheme.

the dimer is lengthened by 0.04 Å and the Si−C distance is shortened by 0.029 Å (Si−C = 1.910 Å).

As a brief summary, these results again demonstrate that the differences between the experimental and calculated Si−C distances of **1**, **3**, and **5**−**7** are indeed apparent discrepancies which can be easily explained by intermolecular interactions of the zwitterions with neighboring molecules in the crystal.

Intramolecular Ligand Exchange. In order to get some more information about the dynamic behavior of the λ^5*Si*-trifluorosilicates and λ^5*Si*-tetrafluorosilicates studied experimentally (in this context, see ref 29), further ab initio calculations with the corresponding model molecules **19** and **20** were performed. These investigations are based on the search for further local minima of these species and transition states for their interconversion into each other.

One local minimum for the λ^5*Si*-tetrafluorosilicate **19** (here denoted as **19a**) obtained by geometry optimization has already been described in Description of Chemical Bonding. Further ab initio studies yielded a second local minimum for this molecule (**19b**) which can be best described as a distorted TBP, the axial sites being occupied by a fluorine atom and the carbon atom (see Figure 16).[30] This minimum is more stable than **19a** by 1.0 kJ mol^{-1} at the SCF/SVP level (5.2 kJ mol^{-1} at the MP2/TZP level), which, however, is hardly significant when regarding the methods of theoretical treatment used. For all λ^5*Si*-tetrafluorosilicates studied experimentally, an Si coordination polyhedron related to **19a** was observed in the crystal, with each carbon atom in an equatorial position. As the calculated structures **19a** (equatorial C atom) and **19b** (axial C atom) do not indicate a clear preference of the carbon atom for an equatorial position, we assume packing effects in the crystal to be responsible for this particular type of structure.

The transition energies for two Berry-type pseudorotations of **19** were calculated by localizing the corresponding transition states **19**$^{\ddagger 1}$ and **19**$^{\ddagger 2}$ (see Figure 16).[30] The first process (C atom as the pivotal ligand) involves an exchange of the two axial and the two equatorial fluorine atoms, including a torsion around the Si−C bond. The second process (F(3) as the pivotal ligand) is characterized by the exchange of the two axial fluorine atoms and the carbon atom and one equatorial fluorine atom, again including a torsion around the Si−C bond. The energy barriers for these two ligand exchange processes were calculated to be 19.8 kJ mol^{-1} (**19**$^{\ddagger 1}$) and 7.5 kJ mol^{-1} (**19**$^{\ddagger 2}$), respectively. A third dynamic process of **19** concerns a torsion around the Si−C bond of **19b** (transition state **19**$^{\ddagger 3}$; see Figure 17). This process, in combination with one pseudorotation, allows the exchange of all five ligand atoms bound to silicon. The energy barrier for this torsion around the Si−C bond (24.1 kJ mol^{-1}) is higher than those for the aforementioned pseudorotations but is still relatively low. This is in good agreement with the results of the ^{19}F NMR studies of the λ^5*Si*-tetrafluorosilicates **5**, **6**, and **9**, which were found to undergo a rapid ligand exchange (see NMR Studies at Room Temperature).[31]

For the λ^5*Si*-trifluorosilicate **20**, six local minima (**20a**−**f**; see Figure 18) were found.[32] The most stable structure of **20** (here denoted as **20a**) has already been described in Theoretical Studies: General and Methodical Aspects. This local minimum corresponds to the experimentally established structures of the λ^5*Si*-trifluorosilicates **7**, **8**, and **10**. The local minimum **20b** (relative energy 4.0 kJ mol^{-1}) is energetically very similar to **20a**, whereas the structures **20c**−**f** are significantly less stable (relative energy 15.0−66.6 kJ mol^{-1}). The energy difference between **20b** and **20d** shows that the effect of the torsion around the Si−C(2) bond is comparable to the energy effect observed for the pseudorotation processes at the silicon atom. A methyl group in an axial position (**20c**,**e**,**f**) leads to an energetic destabilization. Torsion around the Si−C(2) bond (**20a** → **20a′**; transition state **20**$^{\ddagger 1}$; see Figure 19)[33] leads to an exchange of the two axial fluorine atoms F(1) and F(2). The calculated energy barrier for this ligand exchange process amounts to 25.6 kJ mol^{-1}; the relative energy of a second possible transition state (**20**$^{\ddagger 2}$; 48.6 kJ mol^{-1}) for the conversion **20a** → **20a′** was calculated to be significantly higher.[33] Although the calculated value of 25.6 kJ mol^{-1} is distinctly lower than the

(28) Calculated energies (hartree) (additional p function for H): monomeric **19**, −782.660 86 (C_s symmetry); dimeric **19**, −1565.392 54 (C_i symmetry). Selected geometric data (distances in Å, angles in deg) for dimeric **19** and differences (in parentheses) to monomeric **19**: Si−F(1), 1.726 (0.04); Si−F(2), 1.624 (−0.011); Si−F(3), 1.589 (−0.004); Si−F(4), 1.613 (0.02); Si−C, 1.910 (−0.029); F(1)−Si−F(2), 176.5 (3.9); F(1)−Si−F(3), 89.0 (−1.5); F(1)−Si−F(4), 86.9 (−3.6); F(1)−Si−C, 88.4 (1.8); F(2)−Si−F(3), 94.1 (0.7); F(2)−Si−F(4), 93.1 (−0.7); F(2)−Si−C, 88.6 (2.6); F(3)−Si−F(4), 117.7 (−1.9); F(3)−Si−C, 121.4 (0.8); F(4)−Si−C, 120.9 (0.7).

(29) Review on S_N reactions at silicon: Janzen, A. F. *Coord. Chem. Rev.* **1994**, *130*, 355−426.

(30) Calculated energies (hartree): **19a**, −782.607 82 (C_s symmetry); **19b**, −782.608 20 (C_s symmetry); **19**$^{\ddagger 1}$, −782.600 27 (C_s symmetry); **19**$^{\ddagger 2}$, −782.605 36 (C_1 symmetry); **19**$^{\ddagger 3}$, −782.599 02 (C_s symmetry). Calculated energies (hartree) at the MP2/TZP level (SCF energy + single point MP2 energy): **19a**, −783.823 68; **19b**, −783.825 66. Selected geometric data (distances in Å, angles in deg; SCF/SVP level) for **19b**: Si−F(1/3), 1.625; Si−F(2), 1.602; Si−F(4), 1.609; Si−C, 1.983; F(1/3)−Si−F(2), 124.1; F(1)−Si−F(3), 111.1; F(1/3)−Si−F(4), 92.8; F(1/3)−Si−C, 86.9; F(2)−Si−F(4), 92.6; F(2)−Si−C, 87.9; F(4)−Si−C, 179.6.

(31) For **5**, **6**, and **9**, even at low temperature (−80 °C), only one ^{19}F NMR signal could be detected.

(32) Six local minima with the following energies (hartree) were found at the SCF/SVP level: **20a**, −722.692 10 (C_1 symmetry); **20b**, −722.690 56 (C_s symmetry); **20c**, −722.686 37 (C_s symmetry); **20d**, −722.683 94 (C_1 symmetry); **20e**, −722.679 74 (C_1 symmetry); **20f**, −722.666 73 (C_s symmetry). Local minima at the MP2/SVP level (SCF energy + single point MP2 energy) (hartree): **20a**, −722.817 57; **20b**, −722.815 25; **20c**, −722.811 70; **20d**, −722.808 95; **20e**, −722.807 32; **20f**, −722.791 33. All Si−F bonds are longer at the MP2/SVP level by 0.013−0.065 Å (average value 0.030(12) Å), whereas the Si−C bonds are shorter by 0.006−0.028 Å (average value 0.016(9) Å).

(33) Calculated energies (SCF + single point MP2 + E_{vib0}) (hartree): **20**$^{\ddagger 1}$, −782.682 36 (C_1 symmetry); **20**$^{\ddagger 2}$, −782.673 58 (C_s symmetry).

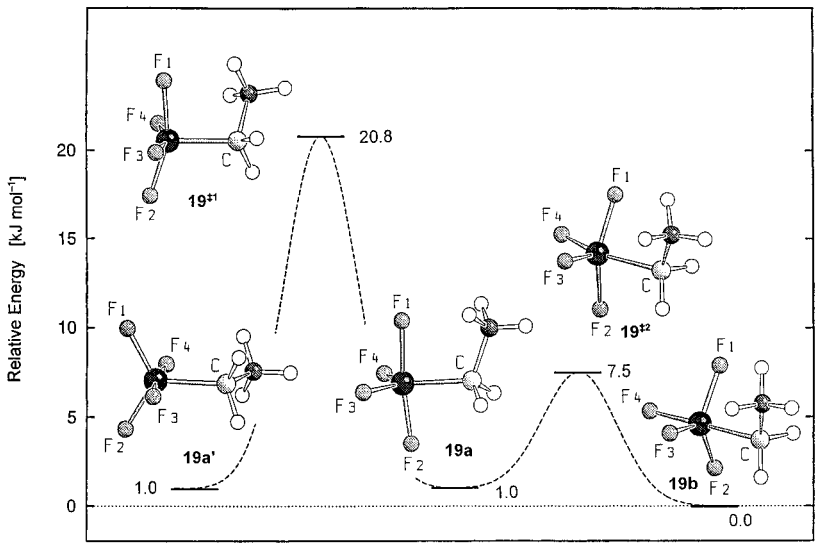

Figure 16. Structures of the calculated minima (**19a**/**19a′**, **19b**) and transition states (**19**‡1, **19**‡2) of the Berry pseudorotation for **19** and their corresponding relative energies.

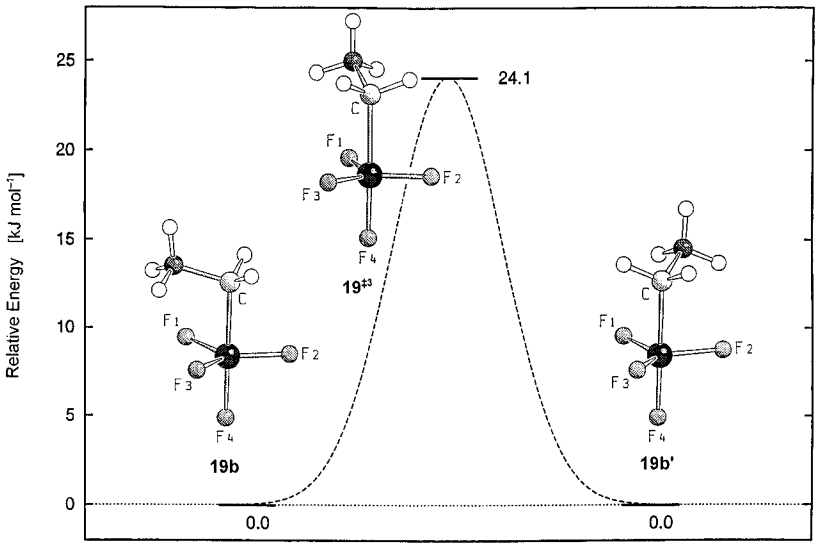

Figure 17. Calculated transition state **19**‡3 for the intramolecular ligand exchange of all ligands of **19** (torsion around the Si−C bond of **19b**).

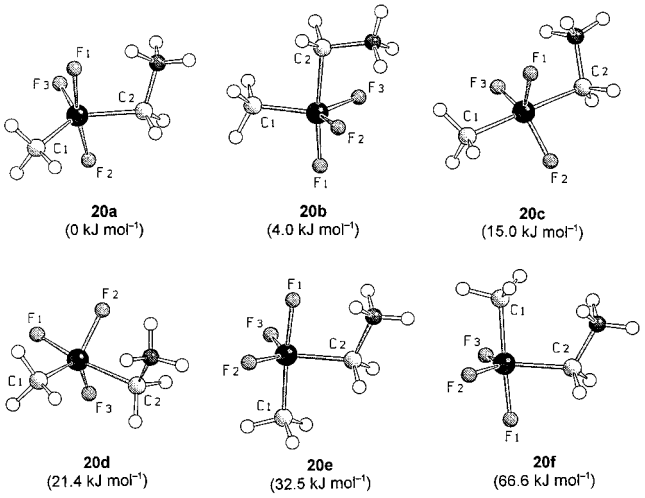

Figure 18. Structures of the calculated local minima (**20a**−**f**) for **20** and their corresponding relative energies.

experimentally established activation energy for the torsion around the Si−C(2) bond of **10** (40.9 kJ mol^{-1}; see Temperature-Dependent ^{19}F NMR Studies of **10**), this result can also be regarded as an acceptable agreement between theory and experiment. Since the 2,2,6,6-tetramethylpiperidinio moiety of **10** is much bulkier than the ammonio group of **20**, a significantly higher energy barrier for the torsion around the Si−C(2) bond has to be expected for **10**.

For the exchange of all five ligand atoms bound to silicon, two pathways were determined (see Figures 20 (pathway 1) and 21 (pathway 2)). For pathway 2, only the SCF energies can be given.[34] The energy differences between these two pathways are not significant when regarding the methods of theoretical treatment used, so that both possibilities have to be considered. The calculated transition energies amount to 42.1 kJ mol^{-1}

(34) Calculated energies (hartree) for pathway 1: **20**‡3, −782.686 25 (C_1 symmetry); **20**‡4, −782.676 06 (C_s symmetry). Calculated SCF energies (hartree) for pathway 2: **20a**, −721.799 01 (C_1 symmetry); **20b**, −721.799 10 (C_s symmetry); **20d**, −721.792 83 (C_1 symmetry); **20e**, −721.788 40 (C_1 symmetry); **20**‡5, −721.791 65 (C_1 symmetry); **20**‡6, −781.789 66 (C_1 symmetry); **20**‡7, −781.787 37 (C_1 symmetry); **20**‡8, −781.786 08 (C_1 symmetry). For pathway 2, addition of the single-point MP2 energy stabilizes the transition states **20**‡5 and **20**‡7 more than the related minima **20d** and **20e**, so that the energies of **20**‡5 and **20**‡7 are dropped below those of **20d** and **20e**. Therefore, for pathway 2 only the corresponding SCF energies are given.

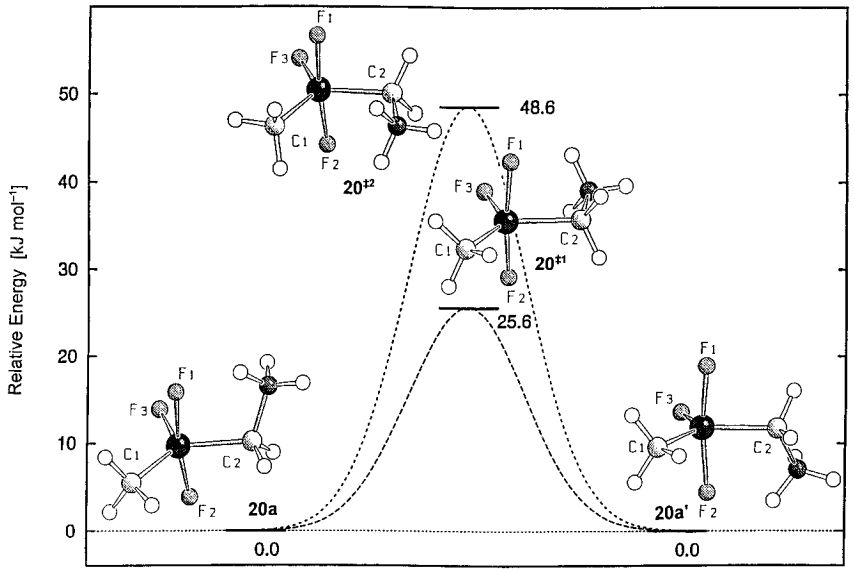

Figure 19. Calculated pathways for the torsion around the Si−C(2) bond of **20** (**20a** ⇌ **20a′**) via the transition state **20**^{‡1} or **20**^{‡2}.

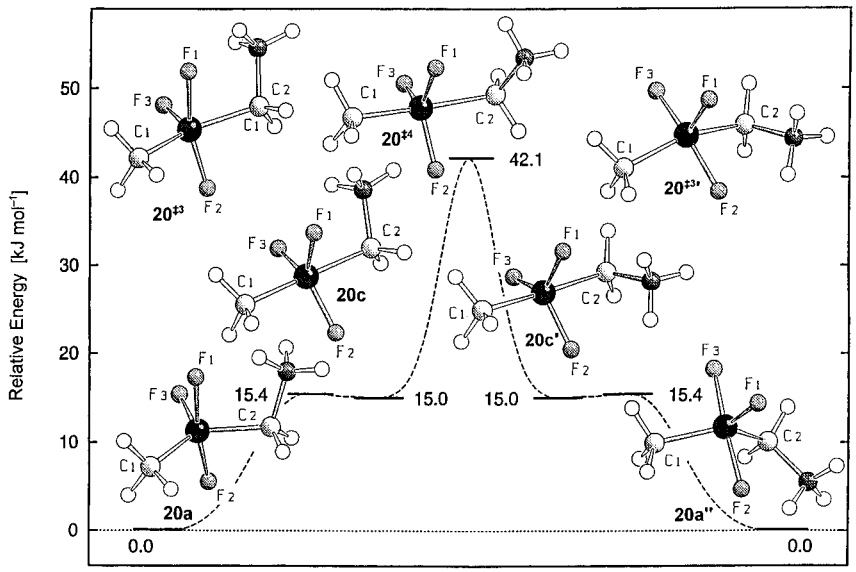

Figure 20. Calculated intramolecular ligand exchange of **20** via the local minimum **20c** and the transition states **20**^{‡3} and **20**^{‡4} (pathway 1).

(pathway 1) and 34.2 kJ mol^{-1} (pathway 2), respectively. These transition energies are in good agreement with the activation enthalpy of 44.4 kJ mol^{-1} obtained by the temperature-dependent ^{19}F NMR studies of **10**. Thus, the experimentally established dynamic behavior of **10** can be well described on the basis of the intramolecular ligand exchange processes shown for the model molecule **20** in Figures 19−21.

The calculated pathways for **19** and **20** show that not only the Berry pseudorotation at the pentacoordinate silicon atom (as observed for smaller anionic species of the formula type $[F_4SiR]^-$ and $[F_3SiR_2]^-$) has to be considered when describing intramolecular dynamic processes of the title compounds: for the zwitterions studied, the torsion around the Si−C bond of the ammoniomethyl fragment is also important.

Conclusions. Zwitterionic λ^5*Si*-organofluorosilicates of the formula types $F_4SiCH_2NMe_2R$ and $F_3MeSiCH_2NMe_2R$ (R = H, Me) and related compounds were studied by both experimental and theoretical methods. The results obtained demonstrate the great efficiency of joint experimental and theoretical investigations which provide complementary information leading to a consistent and more detailed picture of the structure and dynamic behavior of the title compounds.

Experimental Section

General Procedures. Except for the reactions with hydrofluoric acid, all syntheses were carried out under dry nitrogen. The solvents used were dried according to standard procedures and stored under nitrogen. The reactions with hydrofluoric acid were carried out in polypropylene or Nalgene beakers under normal atmospheric conditions; for filtrations polypropylene suction flasks, polypropylene Büchner funnels, and normal commercial filter paper were used. Melting points were determined with a Leitz Laborlux S microscope, equipped with a heater (Leitz, Model M 350). The ^{1}H, ^{13}C, ^{19}F, and ^{29}Si solution-state NMR spectra (room temperature) were recorded on a Bruker AC-250 NMR spectrometer (^{1}H, 250.1 MHz; ^{13}C, 62.9 MHz; ^{19}F, 235.4 MHz; ^{29}Si, 49.7 MHz). $CDCl_3$, CD_2Cl_2, CD_3CN, and CD_3NO_2 were used as solvents. Chemical shifts (ppm) were determined relative to internal $CHCl_3$ (^{1}H, δ 7.25; $CDCl_3$), $CDCl_3$ (^{13}C, δ 77.05; $CDCl_3$), $CDHCl_2$ (^{1}H, δ 5.31; CD_2-

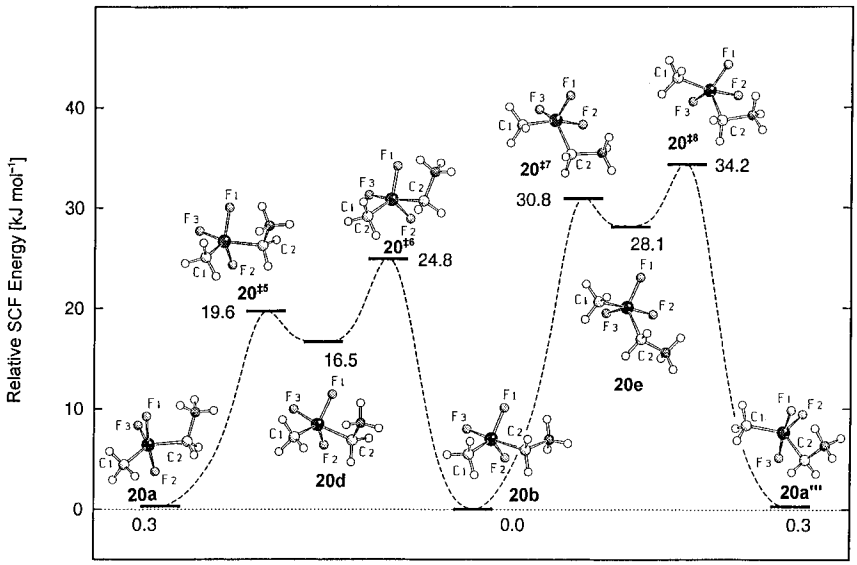

Figure 21. Calculated intramolecular ligand exchange of **20** via the local minima **20b**,**d**,**e** and the transition states **20**‡5, **20**‡6, **20**‡7, and **20**‡8 (pathway 2). The energy values given[34] and the numbering schemes used do not correspond to Figure 18.

Cl_2), CD_2Cl_2 (^{13}C, δ 55.7; CD_2Cl_2), CD_2HCN (^1H, δ 1.93; CD_3CN), CD_3CN (^{13}C, δ 1.30; CD_3CN), CD_2HNO_2 (^1H, δ 4.33; CD_3NO_2), CD_3NO_2 (^{13}C, δ 62.8; CD_3NO_2) and relative to internal TMS (^{29}Si, δ 0) and $CFCl_3$ (^{19}F, δ 0). Assignment of the ^{13}C NMR data was supported by DEPT experiments. High-resolution solid-state ^{29}Si NMR spectra were obtained on a Bruker MSL-300 NMR spectrometer operating at 59.6 MHz, the chemical shifts (ppm) being determined relative to external TMS (^{29}Si, δ 0) (for further experimental details, see also ref 2g). Mass spectra were obtained with a Varian MAT-711 (EI MS, 70 eV; FD MS, 11 kV, for the liquid matrix, see Experimental Section). The selected *m*/*z* values given refer to the isotopes ^1H, ^{12}C, ^{14}N, ^{19}F, and ^{28}Si. Elemental analyses were determined by Beller Mikroanalytisches Laboratorium (Göttingen, Germany). The starting materials [(dimethylamino)methyl]trimethoxysilane (**11**),[2g] [(dimethylamino)methyl]dimethoxy(methyl)silane (**13**),[2g] and (chloromethyl)trimethoxysilane (**15**)[10] were prepared according to published procedures.

Preparation of [(Dimethylammonio)methyl]tetrafluorosilicate (5). A solution of **11** (1.00 g, 5.58 mmol) in ethanol (4 mL) was added dropwise at 0 °C over 1 min to a stirred solution of 40% hydrofluoric acid (1.40 g, 28.0 mmol of HF) in ethanol (7 mL) (spontaneous formation of a precipitate). After the reaction mixture was stirred at 0 °C for 2 h, the precipitate was filtered off and recrystallized from methanol (cooling of a saturated (20 °C) solution to −30 °C) to give compound **5** in 83% yield as a colorless, crystalline product (760 mg, 4.66 mmol): sublimes at >150 °C; mp 162 °C. ^1H NMR (CD_3CN): δ 2.61 (s, 2 H, $SiCH_2N$), 2.76 (s, 6 H, NCH_3), 6.3−6.9 (m, 1 H, NH). ^{13}C NMR (CD_3CN): δ 47.1 (NCH_3), 50.6 ($SiCH_2N$). ^{19}F NMR (CD_3CN): δ −121.7 (s). ^{29}Si NMR (CD_3CN): δ −123.8. ^{29}Si CP/MAS NMR (spinning rate 3775 Hz, 1162 transients, contact time 5 ms, recycle delay time 5 s): δ −120.6 ($\nu_{1/2} \approx$ 475 Hz). EI MS: *m*/*z* 143 [31%, $(M - HF)^+$], 58 [100%, $CH_2{=}N(CH_3)_2^+$]. Anal. Calcd for $C_3H_9F_4NSi$: C, 22.08; H, 5.56; F, 46.57; N, 8.58. Found: C, 22.3; H, 5.6; F, 46.4; N, 8.5.

Preparation of Tetrafluoro[(trimethylammonio)methyl]silicate (6). Methyl iodide (7.95 g, 56.0 mmol) was added dropwise at room temperature over 10 min to a stirred solution of **11** (1.67 g, 9.31 mmol) in acetonitrile (50 mL) and the mixture then heated under reflux for 3 h. After the solvent and excess methyl iodide were removed under reduced pressure, the residue was washed with acetonitrile (5 mL) and then dried in vacuo (0.05 Torr, room temperature, 2 h) to give compound **12** (3.00 g) as a solid crude product. A solution of **12** (3.00 g, crude product) in ethanol (25 mL) was added dropwise at 0 °C over 10 min to a stirred solution of 40% hydrofluoric acid (2.50 g, 50.0 mmol of HF) in ethanol (25 mL) (first crystals formed after about 1 min). After the reaction mixture was stirred at 0 °C for 2 h, the precipitate was filtered off and then recrystallized from acetonitrile (cooling of a saturated (20 °C) solution to −30 °C) to give compound **6** in 87% yield (relative to **11**) as a colorless, crystalline product (1.44 g, 8.13 mmol): mp 216 °C. ^1H NMR (CD_3CN): δ 2.87 (s, 2 H, $SiCH_2N$), 3.08 (s, 9 H, NCH_3). ^{13}C NMR (CD_3CN): δ 56.6 (NCH_3), 59 (m, $SiCH_2N$). ^{19}F NMR (CD_3CN): δ −116.6 (s). ^{29}Si NMR (CD_3CN): experiment failed. ^{29}Si CP/MAS NMR (spinning rate 3947 Hz, 1457 transients, contact time 5 ms, recycle delay time 5 s): δ −122.8. EI MS: *m*/*z* 158 [40%, $M^+ - F$], 58 [100%, $CH_2{=}N(CH_3)_2^+$]. FD MS (CH_3CN): *m*/*z* 158 [100%, $M^+ - F$]. Anal. Calcd for $C_4H_{11}F_4NSi$: C, 27.11; H, 6.26; F, 42.88; N, 7.90. Found: C, 27.3; H, 6.4; F, 42.7; N, 7.9.

Preparation of [(Dimethylammonio)methyl]trifluoro(methyl)silicate (7): Modification 7a. A solution of **13** (1.00 g, 6.12 mmol) in ethanol (4 mL) was added dropwise at 0 °C over 1 min to a stirred solution of 40% hydrofluoric acid (1.25 g, 25.0 mmol of HF) in ethanol (7 mL) (first crystals formed after about 10 min). After the reaction mixture was stirred at 0 °C for 2 h, the precipitate was filtered off and recrystallized from methanol (cooling of a saturated (20 °C) solution to −30 °C) to give compound **7a** in 72% yield as a colorless, crystalline product (700 mg, 4.40 mmol): mp 134 °C. ^1H NMR (CD_3CN): δ −0.01 (s, 3 H, $SiCH_3$), 2.45 (s, 2 H, $SiCH_2N$), 2.77 (s, 6 H, NCH_3), NH resonance not resolved. ^{13}C NMR (CD_3CN): δ 47.1 (NCH_3), 54.3 ($SiCH_2N$), $SiCH_3$ resonance not detected (overlapping with the reference signal). ^{19}F NMR (CD_3CN): δ −104.0 (broad s, $\nu_{1/2} \approx$ 1135 Hz). ^{29}Si NMR (CD_3CN): experiment failed. EI MS: *m*/*z* 139 [12%, $(M - HF)^+$], 58 [100%, $CH_2{=}N(CH_3)_2^+$]. Anal. Calcd for $C_4H_{12}F_3NSi$: C, 30.17; H, 7.60; F, 35.80; N, 8.80. Found: C, 30.3; H, 7.8; F, 35.7; N, 8.9.

Preparation of [(Dimethylammonio)methyl]trifluoro(methyl)silicate (7): Modification 7b. A saturated solution of **7a** in ethanol was slowly (12 h) cooled from 40 °C to 20 °C to give compound **7b** as a colorless, crystalline solid: mp 152 °C. The NMR and MS data of **7b** were identical with those described for **7a** (see above).

Preparation of Trifluoro(methyl)[(trimethylammonio)methyl]silicate (8). Methyl iodide (1.40 g, 9.86 mmol) was added dropwise at room temperature over 10 min to a stirred solution of **13** (268 mg, 1.64 mmol) in acetonitrile (20

mL) and the mixture then heated under reflux for 3 h. After the solvent and excess methyl iodide were removed under reduced pressure, the residue was washed with acetonitrile (5 mL) and then dried in vacuo (0.05 Torr, room temperature, 2 h) to give 500 mg of **14** as a solid crude product. A solution of **14** (500 mg of crude product) in ethanol (5 mL) was added dropwise at 0 °C over 1 min to a stirred solution of 40% hydrofluoric acid (330 mg, 6.60 mmol of HF) in ethanol (7 mL). The reaction mixture was stirred at 0 °C for 2 h and then kept at −30 °C for 16 h. The precipitate was filtered off and recrystallized from ethanol (cooling of a saturated (20 °C) solution to −30 °C) to give compound **8** in 81% yield (relative to **13**) as a colorless, crystalline product (230 mg, 1.33 mmol): decomposes at >145 °C. ^{1}H NMR (CD_3CN): δ −0.09 (m, 3 H, $SiCH_3$), 3.11 (s, 2 H, $SiCH_2N$), 3.11 (s, 9 H, NCH_3). ^{13}C NMR (CD_3CN): δ 56.0 (NCH_3), 56.1 ($SiCH_2N$), $SiCH_3$ resonance not detected (overlapping with the reference signal). ^{19}F NMR (CD_3CN): δ −109.8 (s, $^1J_{SiF}$ = 216.6 Hz). ^{29}Si NMR (CD_3CN, INEPT): experiment failed. EI MS: *m/z* 153 [1%, $(M - HF)^+$], 58 [100%, $CH_2{=}N(CH_3)_2^+$]. Anal. Calcd for $C_5H_{14}F_3NSi$: C, 34.66; H, 8.14; F, 32.90; N, 8.08. Found: C, 35.0; H, 8.2; F, 33.2; N, 8.1.

Preparation of Tetrafluoro[(2,2,6,6-tetramethylpiperidinio)methyl]silicate (9). A solution of **16** (550 mg, 2.00 mmol) in ethanol (7 mL) was added dropwise at 0 °C over 1 min to a stirred solution of 40% hydrofluoric acid (500 mg, 10.0 mmol of HF) in ethanol (10 mL) (spontaneous formation of a precipitate). After the reaction mixture was stirred at 0 °C for 2 h, the precipitate was filtered off and recrystallized from acetonitrile (cooling of a saturated (20 °C) solution to −30 °C) to give compound **9** in 95% yield as a colorless, crystalline product (490 mg, 1.89 mmol): sublimes at >240 °C; mp 271 °C. ^{1}H NMR (CD_3CN): δ 1.34 (s, 6 H, $NCCH_3$), 1.36 (s, 6 H, $NCCH_3$), 1.55−1.9 (m, 6 H, CCH_2C), 2.55−2.60 (m, 2 H, $SiCH_2N$), 5.7−6.2 (m, 1 H, NH). ^{13}C NMR (CD_3CN): δ 16.4 ($NCCCH_2C$), 20.0 ($NCCH_3$), 30.1 ($NCCH_3$), 35.9 (quint, $^2J_{CF}$ = 40.6 Hz, $SiCH_2N$), 39.2 ($NCCH_2C$), 65.9 ($NCCH_3$). ^{19}F NMR (CD_3CN): δ −123.2 (s, $^1J_{SiF}$ = 203.8 Hz). ^{29}Si NMR (CD_3CN, INEPT): δ −123.5 (quint, $^1J_{SiF}$ = 204.4 Hz). EI MS: *m/z* 239 [2%, $(M - HF)^+$], 155 [100%, $CH_2{=}NC_9H_{19}^+$]. FD MS (CH_3CN): *m/z* 239 [100%, $(M - HF)^+$], 155 (33%, $CH_2{=}NC_9H_{19}^+$]. Anal. Calcd for $C_{10}H_{21}F_4NSi$: C, 46.31; H, 8.16; F, 29.30; N, 5.40. Found: C, 46.6; H, 8.2; F, 29.0; N, 5.5.

Preparation of *tert*-Butyltrifluoro[(2,2,6,6-tetramethylpiperidinio)methyl]silicate (10). A solution of **17** (3.02 g, 10.0 mmol) in ethanol (10 mL) was added dropwise at 0 °C over 5 min to a stirred solution of 40% hydrofluoric acid (2.00 g, 40.0 mmol of HF) in ethanol (10 mL). The reaction mixture was stirred at 0 °C for 2 h and then kept at −30 °C for 16 h. The precipitate was filtered off and recrystallized from ethanol (cooling of a saturated (20 °C) solution to −30 °C) to give compound **10** in 68% yield as a colorless, crystalline product (2.02 g, 6.79 mmol): sublimes at >145 °C; mp 201 °C. ^{1}H NMR (CD_3CN): δ 0.91 (q, $^4J_{HF}$ = 1.2 Hz, 9 H, $C(CH_3)_3$), 1.32 (s, 6 H, $NCCH_3$), 1.37 (s, 6 H, $NCCH_3$), 1.5−1.9 (m, 6 H, CCH_2C), 2.40−2.42 (m, 2 H, $SiCH_2N$), 6.0−6.6 (m, 1 H, NH). ^{13}C NMR (CD_3CN): δ 16.6 ($NCCCH_2C$), 20.3 ($NCCH_3$), 31.0 ($NCCH_3$), 30.0 ($C(CH_3)_3$)), 38.7 (q, $^2J_{CF}$ = 44.5 Hz, $SiCH_2N$), 39.7 ($NCCH_2C$), 65.1 ($NCCH_3$), $C(CH_3)_3$ resonance not resolved. ^{19}F NMR (CD_3CN): δ −111.7 (broad s, $\nu_{1/2} \approx$ 4350 Hz). ^{29}Si NMR (CD_3CN, INEPT): δ −93.6 (q, $^1J_{SiF}$ = 261.1 Hz). ^{1}H NMR ($CDCl_3$): δ 1.00 (s, 9 H, $C(CH_3)_3$), 1.35 (s, 6 H, $NCCH_3$), 1.47 (s, 6 H, $NCCH_3$), 1.6−1.9 (m, 6 H, CCH_2C), 2.48−2.49 (m, 2 H, $SiCH_2N$), 6.3−6.7 (broad s, 1 H, NH). ^{13}C NMR ($CDCl_3$): δ 16.6 ($NCCCH_2C$), 20.9 ($NCCH_3$), 31.4 ($NCCH_3$), 23 (m, $C(CH_3)_3$), 30.0 ($C(CH_3)_3$), 38.8 (q, $^2J_{CF}$ = 29.7 Hz, $SiCH_2N$), 39.9 ($NCCH_2C$), 64.7 ($NCCH_3$). ^{19}F NMR ($CDCl_3$): δ −111.8 (broad s, $\nu_{1/2} \approx$ 3780 Hz). ^{29}Si NMR ($CDCl_3$, INEPT): δ −92.7 (q, $^1J_{SiF}$ = 265.7 Hz). ^{1}H NMR (CD_3NO_2): δ 0.91 (m, 9 H, $C(CH_3)_3$), 1.42 (s, 12 H, $NC(CH_3)_2$), 1.6−2.0 (m, 6 H, CCH_2C), 2.44 (s, 2 H, $SiCH_2N$), NH resonance not resolved. ^{13}C NMR (CD_3NO_2): δ 16.9 (CCH_2C), 20.3 ($NCCH_3$), 31.2 ($NCCH_3$), 23.8 (m, $C(CH_3)_3$), 30.0 (CCH_3), 38.6 (m, $SiCH_2N$), 39.9 ($NCCH_2C$), 65.5 ($NCCH_3$). ^{19}F NMR (CD_3NO_2): δ −114.7. ^{29}Si NMR (CD_3NO_2, INEPT): δ −93.1 (q, $^1J_{SiF}$ = 262.9 Hz). ^{1}H NMR (CD_2Cl_2): δ 0.90 (s, 9 H, $C(CH_3)_3$), 1.30 (s, 6 H, $NCCH_3$), 1.38 (s, 6 H, $NCCH_3$), 1.5−1.9 (m, 6 H, CCH_2C), 2.37−2.40 (m, 2 H, $SiCH_2N$), 6.0−6.3 (broad s, 1 H, NH). ^{13}C NMR (CD_2Cl_2): δ 16.3 ($NCCCH_2C$), 20.4 ($NCCH_3$), 31.4 ($NCCH_3$), 22.3 (m, $C(CH_3)_3$), 29.6 ($C(CH_3)_3$), 38.7 (m, $SiCH_2N$), 39.6 ($NCCH_2C$), 64.4 ($NCCH_3$). ^{19}F NMR (CD_2Cl_2): see Temperature-Dependent ^{19}F NMR Studies. ^{29}Si NMR (CD_2Cl_2, INEPT): δ −93.4 (q, $^1J_{SiF}$ = 264.0 Hz). ^{29}Si CP/MAS NMR (spinning rate 3917 Hz, 1088 transients, contact time 5 ms, recycle delay time 3 s): δ −97.2. EI MS: *m/z* 277 [16%, $(M - HF)^+$], 262 [(100%, $(M - HF - CH_3)^+$], 154 [76%, $CH_2{=}NC_9H_{18}^+$]. Anal. Calcd for $C_{14}H_{30}F_3NSi$: C, 56.53; H, 10.16; F, 19.16; N, 4.71. Found: C, 56.5; H, 10.0; F, 19.4; N, 4.7.

Preparation of Trimethoxy[(2,2,6,6-tetramethylpiperidino)methyl]silane (16). A mixture of **15** (3.38 g, 19.8 mmol) and 2,2,6,6-tetramethylpiperidine (8.39 g, 59.4 mmol) was heated under reflux for 8 h and then stirred for a further 16 h at room temperature. The precipitate was filtered off and washed with *n*-pentane (50 mL), and the filtrate was combined with the washings and the solvent removed by distillation at normal pressure. The residue was distilled in vacuo (Vigreux column) to give compound **16** in 64% yield as a colorless liquid (3.48 g, 12.6 mmol): bp 56 °C/0.01 Torr. ^{1}H NMR ($CDCl_3$): δ 0.95 (s, 12 H, CCH_3), 1.3−1.5 (m, 6 H, CCH_2C), 1.99 (s, 2 H, $SiCH_2N$), 3.55 (s, 9 H, OCH_3). ^{13}C NMR ($CDCl_3$): δ 18.0 ($NCCCH_2C$), 26.4 (CCH_3), 28.3 ($SiCH_2N$), 41.2 ($NCCH_2C$), 51.0 (OCH_3), 54.9 (CCH_3). ^{29}Si NMR ($CDCl_3$): δ −48.6. EI MS: *m/z* 275 [6%, M^+], 260 [100%, $M^+ - CH_3$], 154 [17%, $CH_2{=}NC_9H_{18}^+$]. Anal. Calcd for $C_{13}H_{29}NO_3Si$: C, 56.68; H, 10.61; N, 5.08. Found: C, 56.8; H, 10.8; N, 5.2.

Preparation of *tert*-Butyldimethoxy[(2,2,6,6-tetramethylpiperidino)methyl]silane (17). A 1.7 M solution of *tert*-butyllithium in *n*-pentane (5.88 mL, 10.0 mmol of *t*-BuLi) was added dropwise at −30 °C over 1 h to a stirred solution of **16** (2.50 g, 9.08 mmol) in *n*-pentane (50 mL). The mixture was heated under reflux for 3 h and then stirred for a further 12 h at room temperature. The precipitate was filtered off, the solvent removed under reduced pressure, and the residue distilled in vacuo (Vigreux column) to give compound **17** in 64% yield as a colorless liquid (1.76 g, 5.84 mmol): bp 110 °C/0.04 Torr. ^{1}H NMR ($CDCl_3$): δ 0.93 (s, 9 H, $C(CH_3)_3$), 1.01 (s, 12 H, $NC(CH_3)_2$), 1.4−1.6 (m, 6 H, CCH_2C), 2.03 (s, 2 H, $SiCH_2N$), 3.70 (s, 6 H, OCH_3). ^{13}C NMR ($CDCl_3$): δ 18.1 ($NCCCH_2C$), 20.4 ($C(CH_3)_3$), 26.6 ($C(CH_3)_3$), 26.9 ($NC(CH_3)_2$), 29.5 ($SiCH_2N$), 41.6 ($NCCH_2C$), 52.0 (OCH_3), 55.1 ($NC(CH_3)_2$). ^{29}Si NMR ($CDCl_3$, INEPT): δ −15.8 (s). EI MS: *m/z* 301 [9%, M^+], 286 [28%, $M^+ - CH_3$], 154 [100%, $CH_2{=}NC_9H_{18}^+$]. Anal. Calcd for $C_{16}H_{35}NO_2Si$: C, 63.73; H, 11.70; N, 4.65. Found: C, 63.9; H, 11.8; N, 4.7.

Crystal Structure Analyses. Cell parameters were obtained from least-squares fits to the settings of 25 reflections in the range $15° \le \theta \le 20°$ centered on a Siemens P4 diffractometer by using Mo Kα radiation. Intensities were collected for colorless, prismatic crystals at −110 °C (**5**, **6**) or −100 °C (**7a**,**b**, **8**−**10**) for $2\theta \le 60°$. No significant deviations in intensity were registered for three monitor reflections recorded at regular intervals. The structures were solved by direct methods and refined by full-matrix least squares, using the program SHELXTL PLUS with anisotropic thermal parameters for all non-hydrogen atoms.[35] Neutral-atom scattering factors, corrected for the real and imaginary parts of anomalous dispersion, were taken from ref 36. Corrections for absorption for **7a**,**b**, **8**, and **10** were applied after isotropic

(35) Sheldrick, G. M. SHELX-76; University of Cambridge, Cambridge, England. SHELXTL PLUS; Siemens Analytical X-ray Instruments Inc., 1990.

(36) *International Tables for X-Ray Crystallography*; Kynoch Press: Birmingham, England, 1974; Vol. IV, pp 99−149.

least-squares refinement for the non-hydrogen atoms by use of the program DIFABS.[37] Corrections for extinction for **5** were applied with $F_{corr} = F[1 + 0.002\chi F^2/(\sin 2\theta)]^{-1/4}$ with $\chi = 0.0024(2)$. All the hydrogen atoms were located in difference Fourier syntheses and their positions included in the least-squares refinement together with isotropic displacement parameters. The function minimized during the refinement was $\sum w(|F_o| - |F_c|)^2$ with $w = [\sigma^2(F_o) + pF_o^2]^{-1}$, with $p = 0.000\ 01$ (**6**), 0 (**5**, **7a**,**b**), 0.0001 (**8**, **9**), or 0.0004 (**10**). Complete numerical details are given in Tables 1−3 and selected bond distances and angles in Tables 4−7. The atomic coordinates and equivalent isotropic displacement parameters for **6**, **7a**,**b**, and **8**−**10** are listed in Tables 15−21 (Supporting Information). The atomic numbering schemes are given in Figures 1−6. Tables of anisotropic thermal parameters, atomic coordinates for the hydrogen atoms, and complete lists of bond distances and angles are provided as Supporting Information.

Temperature-Dependent ^{19}F NMR Studies of 10. ^{1}H and ^{19}F solution-state NMR spectra of **10** were recorded on a Bruker AMX 300 (^{1}H, 300.1 MHz; ^{19}F, 284.4 MHz). The simulation of the ^{19}F NMR spectra was carried out on an IBM RS 6000 using the iterative computer program DNMR5.[12]

Acknowledgment. We would like to thank Priv.-Doz. Dr. A. Sebald, Bayerisches Geoinstitut/Universität Bayreuth, Germany, for performing the ^{29}Si CP/MAS NMR experiments. Financial support of this work by the Deutsche Forschungsgemeinschaft and the Fonds der Chemischen Industrie is gratefully acknowledged. In addition, we thank Bayer AG (Leverkusen and Wuppertal-Elberfeld, Germany) for gifts of chemicals.

Supporting Information Available: Tables of anisotropic thermal parameters, atomic coordinates, and all bond distances and angles for **5**, **6**, **7a**,**b**, and **8**−**10** (30 pages). Ordering information is given on any current masthead page.

OM9509296

(37) Walker, N.; Stuart, D. *Acta Crystallogr.* **1983**, *A39*, 158−166.